The Thesis Committee for Gregory Robert Enenstein certifies that this is the approved version of the following thesis:

Two Studies on the Acoustics of Multiphase Materials: Seagrass Tissue and Encapsulated Bubbles

APPROVED BY

SUPERVISING COMMITTEE:

Preston S. Wilson, Supervisor

Kevin M. Lee

Two Studies on the Acoustics of Multiphase Materials: Seagrass Tissue and Encapsulated Bubbles

by

Gregory Robert Enenstein, B.S.

THESIS

Presented to the Faculty of the Graduate School of

The University of Texas at Austin

in Partial Fulfillment

of the Requirements

for the Degree of

MASTER OF SCIENCE IN ENGINEERING

THE UNIVERSITY OF TEXAS AT AUSTIN

May 2014

Dedicated to my father Robert Enenstein.

Acknowledgments

I wish to thank Preston Wilson, Kevin Lee, Craig Dolder, Ted Argo, Mustafa Abbasi, Joelle Suits, Laura Tseng, and Adrienne McCarty, all of whom were immensely helpful during the experimental and/or writing stage of this report. I would also like to thank Bonnie Schnitta, Charles Wiseman, and Thomas Rossing who helped convince me to venture into the field of acoustics.

Two Studies on the Acoustics of Multiphase Materials: Seagrass Tissue and Encapsulated Bubbles

Gregory Robert Enenstein, M.S.E.
The University of Texas at Austin, 2014

Supervisor: Preston S. Wilson

There are two focal points of this thesis: the acoustics of seagrass and the acoustical properties of encapsulated bubbles for underwater noise abatement. The acoustical properties of seagrass have applications in mine hunting, shallow water sonar, and environmental acoustic remote sensing. In order to optimize these applications, a predictive model of acoustic propagation in seagrass beds is sought. Previous laboratory research has indicated that the tissue acoustic properties of seagrass as well as the tissue physical structure and entrained air masses inside the leaves contribute to the overall acoustic behavior. The present research utilized a glass laboratory resonance tube to find the low frequency (1 kHz–4 kHz) acoustic compressibility of two species of seagrass, *Thalassia testidinum* and *Halodule wrightii*. By using a mixture of finely divided seagrass tissue suspended in seawater, the bulk moduli of the seagrass species were extracted. In the second section, encapsulated bubbles were analyzed as a method of abating underwater anthropogenic noise sources,

since these sources, including marine piledriving and oil and gas exploration and production, pose potential harmful effects to marine life. Previous research, which used an array of rubber-shelled encapsulated bubbles, found the attenuation from these bubbles in be in close accordance with an existing encapsulated bubble model. Experiments were performed in a small laboratory resonance tank, a large outdoor acoustic tank, and at Lake Travis Test Station (LTTS) in order to determine the effects of varying an encapsulated bubble's wall thickness and fill material on bubble resonance frequency and damping. Results found that increasing the wall thickness tended to increase the balloon resonance frequencies measured in the small tank, which was strongly correlated to the frequency of maximum noise reduction in the large outdoor test tank and LTTS tests. The addition of polyester fibers and aluminum wool as fill materials decreased both the resonance frequency and quality factor, whereas helium-filled filled encapsulated bubbles had an increased resonance frequency but decreased quality factor as compared with air-filled bubbles. The resonance quality factor and void fraction further proved to affect the noise reduction near bubble resonance in the outdoor acoustic tank and LTTS tests. The measurements made with a single bubble in a small laboratory tank were correlated to measurements with a full-size system composed of many bubbles operating in open water.

Table of Contents

List of Tables

List of Figures

Chapter 1

Introduction

1.1 Background and Motivation

This thesis describes two separate but related studies: characterization of the low-frequency acoustic properties of two species of seagrass in a glass resonator tube, and investigation of the resonance and sound dampening properties of encapsulated bubbles through experiments in a resonance tank, a large outdoor acoustic test tank, and open water tests at Lake Travis Test Station. These two studies are presented as separate analyses that are self-contained in their respective sections. Although these two substories are noncontinuous, both have applications to underwater sound propagation. Seagrass causes attenuation and backscatter of acoustic signals, and by better characterizing the material's acoustic properties, it is possible to improve models for applications including shallow water sonar, mine hunting, and acoustic remote sensing. The main focus for using encapsulated bubbles is the attenuation of anthropogenic noise sources, namely those from pile driving and underwater machinery noise. However, understanding the acoustically attenuative effects of encapsulated bubbles may, like seagrass, be useful for sonar models as well. For example, encapsulated bubbles have been used for models of sonar wave propagation through fish schools [1]. Since the region enclosing an array of

encapsulated bubbles is a mixture of the bubble fill gas, the bubble shell material, and water, and the region around a seagrass bed is a mixture of leaf tissue, bubbles, and water, both it and seagrass can be considered multiphase materials. These experiments sought to achieve increased understanding of the basic acoustic properties within these multiphase materials, which will in turn be useful for future models and applications relating to propagation and attenuation with such materials.

1.2 Road Map of Thesis

Chapter 2 describes an experiment that utilized an acoustic resonator tube to extract the bulk moduli of two species of seagrass. Moreover, it describes the assorted models employed in the experiments, including a two-phase effective medium model, and the relevant acoustic effects that were accounted for in the analysis. Finally, the data is presented and discussed and then manipulated to obtain the bulk moduli, the desired result.

Chapter 3 describes a set of three experiments performed to understand the effects of changing the wall thickness and fill material of encapsulated bubbles on the resonance frequency, quality factor, and ultimately attenuation. The section also compares the results from the different experimental methods and examines if it is possible for the results obtained using a single encapsulated bubble measured inside a small laboratory tank to predict the results measured using a larger number of encapsulated bubbles in a large outdoor test tank and in open water. With each of the three different experiments, the

section describes the methods as well as processes taken to extract the final data. The section concludes with description and analysis of the trends seen in the experiments.

Chapter 4 summarizes the work, provides conclusions and briefly discusses possible future work. Two appendices contain supporting material, including an elastic waveguide model and a collection of MATLAB scripts used to process data presented in the thesis.

Chapter 2

The Acoustics of Seagrass

2.1 Background and Practical Significance

The acoustics of seagrass are important for applications including shallow water sonar, mine hunting, and acoustic remote sensing for ecological studies. Seagrass commonly causes attenuation and backscatter of acoustic signals, which depending on the application can be either detrimental to the overall goal or utilized to determine the presence of seagrass. The effect of seagrass on incident waves has been primarily attributed to the gas-filled regions within the plants (aerenchyma) as well as bubbles in the surrounding regions produced by photosynthesis [2, 3].

Seagrass can have a significant impact on the performance of sonar in shallow water. Lyons and Abraham looked at acoustic backscatter of high frequency shallow water sonar [4]. They measured 80 kHz signals from several distinct shallow bottom regions off the coast of Sardinia and Sicily including sites with *Posidonia oceanica*. They found that the *Posidonia*-covered seafloor had a larger backscatter strength than mud and sand covered bottoms by 0 to 10 dB higher in the *Posidonia* regions as compared to the sand and mud regions.

In addition, McCarthy and Sabol illustrated the effects of backscatter and masking from seagrass while using side scan sonar for mine hunting [5]. Their 100 kHz through 500 kHz range sonars were unable to detect a Manta mine in a meadow of *Zostera marina* in numerous attempts. They concluded that further knowledge of the acoustic properties of seagrass was essential to improving mine hunting performance.

Acoustic remote sensing has been developed as a noninvasive method of performing ecological studies. Seagrass beds play an important role in coastal ecosystems in supporting flora and fauna. Furthermore, they serve as nursery grounds for species, maintain coastal water quality and clarity, and reduce coastal erosion [3, 6]. Therefore, it is important to assess the condition of seagrass meadows.

Several studies in the past 20 years have used acoustic methods to characterize seagrass environments. Mulhearn found that it was possible to relate the prescence of seagrass detected by side scan sonar data to evidence of its existence from aerial photographs [7]. Pasqualini *et al.* used a combination of aerial photographs of seagras beds with side scan sonar imaging [8]. This study used aerial photographs of *Posidonia oceanica* for depths up to 20 m and then side scan sonar from depths of 20-50 m. Lucieer used side scan sonar to create habitat maps to characterize the envionment [9]. Lastly, Komatsu developed a multi-beam sonar scanning method to image a broader area and produce three-dimensional structures [6]. Komatsu's method could estimate the actual volume and biomass of seagrass in a region.

Hermand has conducted several studies with acoustic remote sensing using a waveguide impulse response [3, 10]. The goal of these experiments was to find the affects of photosynthesis on the long range propogation of sound. One such study consisted of sending a signal from 0.1 kHz to 1.6 kHz across a seagrass bed in which photosynthesis created bubble-saturated water throughout the water column above the plants. They subsequently inverted the acoustic data for water column sound speed, related that to gas content through Wood's equation, and related gas content to biomass. In addition, they noted that photosynthesis resulted in increased attenuation and a faster decay of reverberation.

In order to continue to improve and optimize remote sensing, sonar, and mapping applications, accurate forward models of the acoustic propagation and scattering effects in seagrass beds are required. For an entire seabed including the bubbles produced by seagrass, a model that relates plant density, structure, and photosynthetic activity to propagation and scattering would be useful to infer target parameters [2]. However, for simply understanding the basic nature of the acoustics of seagrass, which has been relatively unexplored thus far, two fundamentally important parameters are the bulk density and the compressional wave speed of the plant material itself as compared to the surrounding water [11].

2.2 Previous Studies of Seagrass Acoustic Behavior

Previous research at The University of Texas at Austin was undertaken in order to understand the acoustic behavior of seagrass. In 2006, Wilson and Dunton used a one-dimensional resonator technique to assess the acoustic properties of three species of seagrass: *Thalassia testidinum*, *Syringodium filiforme*, and *Halodule wrightii* [12]. Since the plant tissues were considered to be acoustically close to water, and the gas content within the plants was believed to be acoustically dominant, they used a two-phase effective medium model. By using microscopic imaging, they were able to compare the actual void fraction inside the seagrasses to the apparent acoustic void fraction from Wood's Equation. Wilson and Dunton found that although increasing the number of seagrass leaves in the resonator decreased the overall sound speed of the mixture, Wood's equation alone was not enough to predict the acoustic behavior. In fact, the actual void fraction of air tended to be larger than the acoustic effect that they were seeing. They concluded that the tissue acoustic properties in addition to the gas content had to play a role in the acoustic behavior of seagrass [2].

In 2010 C.J. Wilson *et al.* expanded on these tests by using computed tomography imaging to extract the tissue density and volume [13]. With this additional information, they employed a three-medium model which included the water, the tissue, and the gas inside of the tissue. However, even with this model, they failed to obtain the acoustic compressibility of the seagrass. The study concluded that knowledge of the structure of the tissue was also required

for an accurate propagation model. In summary, previous work has indicated that simply effective medium models of low-frequency sound propagation in seagrass will not work. Hence, full knowledge of both the physical structure and the elastic material properties (bulk and shear moduli) of the plant must be considered.

2.3 Goals

Expanding on the previous studies described in Section 2.2, the experiments described here sought to determine the basic leaf tissue acoustic properties of two species of seagrass: *Thalassia testidinum* (turtle grass) and *Halodule wrightii* (shoal grass). The ultimate target was to find two parameters: first, the sound speed and from that, the bulk modulus of the leaf tissue of each species. By utilizing an experimental method that removed the structure and aerenchyma (air channels) from the seagrass, this approach measured the tissue properties themselves.

2.4 Experimental Setup

The experiment was conducted by taking acoustical measurements in a one-dimensional acoustic resonator tube. The tube was made out of borosilicate glass that was 45.6 cm tall with a circular cross section with a 6.88 cm outer diameter and a 5.09 cm inner diameter. An LDS V10 L shaker was held with a clamp over the tube, with the stinger of the transducer just inside of the tube providing continuously repeated periodic chirps from 50 Hz to 15 kHz

generated by an Agilent 89410A vector signal analyzer (VSA). The acoustic pressure response of the system was acquired with a Reson 4013 hydrophone which was also placed into the top of the tube. The tube itself was filled with the seagrass material and water (preparation described below). The top of the tube was open to the air and the bottom of the tube consisted of a thin latex rubber membrane and a block of styrofoam to allow for approximately pressure release conditions at both ends of the tube.

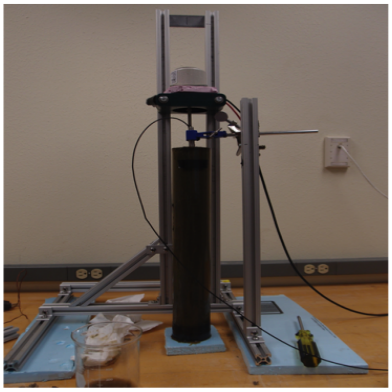

Figure 2.1: Photograph of experimental apparatus.

Sediment core samples containing live plants, sediment, and seawater of *Thalassia testidinum* (turtle grass) and *Halodule wrightii* (shoal grass) were collected less than 24 hours prior to acoustic measurements from shallow waters on the eastern side of Corpus Christi Bay near Port Aransas, TX. The individual leaves were separated from the plants, then samples were weighed and measured for volume by method of water displacement. Each sample was combined with artifical salt water, which was a mix of Instant Ocean and distilled water with a salinity of 35.9 ppt. The resulting mixtures were placed in

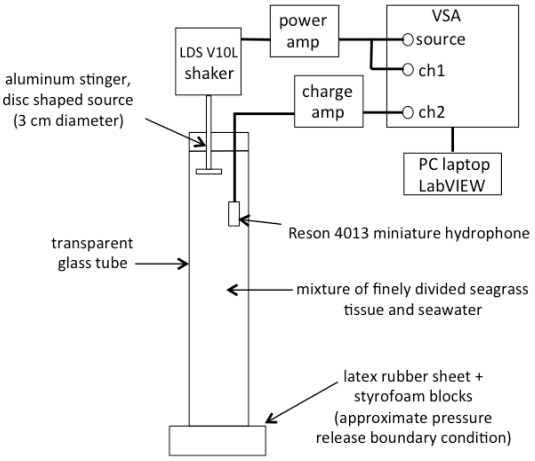

Figure 2.2: Schematic diagram of experimental apparatus, adapted from Enenstein *et al.* 2013 [14].

a food processing blender and broken down until the sample had a consistent composition and the particle size was less than 0.1 mm. It should be noted that the ratio of salt water to seagrass tissue was not identical for the two samples. Since the desired results were the sound speeds and bulk moduli of the tissues themselves, this was completely acceptable because data analysis methods could account for different ratios of seagrass tissue to water between samples. Therefore, readers should be aware that it is not useful to compare the measured sound speed values of the two mixtures themselves. Each sample, or "seagrass soup", was then thoroughly degassed with a stirring rod under a 15 mm Hg vacuum and placed into the glass resonator tube for acoustic measurements. After an initial measurement, measurements were taken at 5 minute intervals for 15 minutes. During this time, there was no visual

stratification and were no visual changes in the composition of the samples.

2.5 Modeling

2.5.1 Extracting the Sound Speed

The tube itself was modeled with perfect pressure release conditions on the top and bottom of the tube. This resulted in a half wavelength of sound inside of the tube at the first resonance frequency of the tube. For every subsequent resonance, there was an additional half wavelength along the length of the tube. Sound speed at the frequency of the n^{th} resonance was found using Equation 2.1:

$$c = f_{\text{res}} \left(\frac{2l_{\text{tube}}}{n} \right). \tag{2.1}$$

The resonance frequencies themselves were determined from the peaks of the measured pressure spectra. Figure 2.4 shows 5 distinct resonance peaks between 1 kHz and 8 kHz in the sample case of a water filled tube.

2.5.2 Elastic Waveguide Effect

Due to significant coupling between the walls of the glass tube and the water inside, there was a reduced sound speed in the tube as compared to the free field sound speed. The elastic waveguide effect was taken into account to extract the free field sound speed. The model used in this study was taken from Del Grosso's 1971 paper [15] which was later explored in the 1995

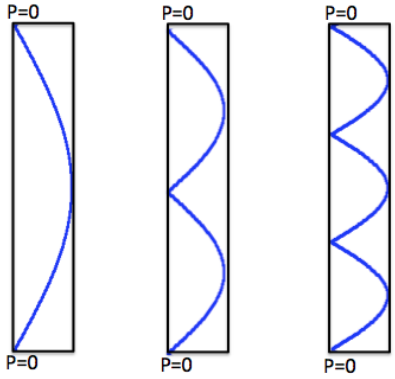

Figure 2.3: Standing wave patterns of the first three modes.

Lafleur and Shields paper [16]. The model provides a dispersion relationship for axisymmetric modes:

$$\begin{aligned}
1 + [L_{11}(P_m)L_{00}(T_m)]\left(\frac{\pi^2 q_{0m}^2 bdP_m^2 T_m^2}{8E_m^2}\right) + [L_{11}(T_m)L_{00}(P_m)\left(\frac{\pi^2 bdE_m^2}{8q_{0m}^2}\right) \\
+[L_{10}(P_m)L_{01}(T_m) + L_{01}(P_m)L_{10}(T_m)] \times \left(\frac{\pi^2 bdP_m T_m}{8}\right) \\
+[bL_{11}(P_m)L_{10}(T_m) + d(1+Q_m b)L_{11}(P_m)L_{01}(T_m)]\left(\frac{\pi^2 P_m^2 T_m}{8E_m} - \frac{\pi^2 P_m^2 q_{0m}^2 T_m}{8E_m^2}\right) \\
+[bL_{11}(T_m)L_{10}(P_m) + d(1+Q_m b)L_{11}(T_m)L_{01}(P_m)]\left(\frac{\pi^2 P_m E_m}{8q_{0m}^2} - \frac{\pi^2 P_m}{8}\right) \\
+[(1+Q_m b)L_{11}(T_m)L_{11}(P_m)]\left(\frac{\pi^2 P_m^2}{8q_{0m}^2} + \frac{\pi^2 P_m^2 q_{0m}^2}{8E_m^2} - \frac{\pi^2 P_m^2}{4E_m}\right) = 0.
\end{aligned} \tag{2.2}$$

The free field sound speed of the fluid within the tube c_0 is an input to Equation 2.2, satisfaction of which yields the admissible modal phase speeds for sound propogation inside the resonance tube. For a full description of the variables used in Equation 2.2, see Appendix A. Only the plane wave mode

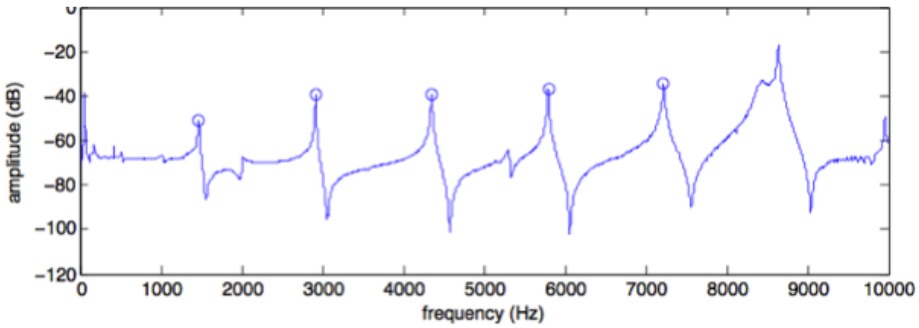

Figure 2.4: Tube response showing resonance peaks. The circled peaks are for longitudinal modes. The pair of peaks between 8 kHz and 9 kHz are a longitudinal acoustic mode and a mechanical resonance of the source piston and its stinger. The smaller resonances near 2 kHz and 5.5 kHz are tube wall flexural resonances.

was used in this work. The value c_0 is varied in Eq. 2.2 until the resulting plane wave modal phase speed matches the measured phase speed from the experiment at each experimental frequency. The value of c_0 that achieves this match is reported as the free-field sound speed of the material in the tube.

2.5.3 Wood's Equation

The material within the resonance tube was a two-phase mixture of artificial ocean water and plant tissue particles. Wood's Equation was used to determine the bulk modulus of the seagrass tissue particles. Wood outlined this equation in 1930, although it is heavily based on an earlier equation for the velocity of a mixed fluid presented by Mallock in 1910 [17, 18]. Wood's Equation utilizes the assumption that the velocity of the mixture is the same as that of a homogenous fluid with the volume-weighted mean density and

bulk modulus of the mixture:

$$c_{\text{eff}} = \sqrt{\frac{B_1 B_2}{[\beta_1 B_2 + (\beta_2) B_1][\beta_1 \rho_1 + \beta_2 \rho_2]}}. \tag{2.3}$$

Here, c_{eff} is the effective sound speed, B_1 is the bulk modulus of material 1, B_2 is the bulk modulus of material 2, β_1 is the volume fraction of material 1, β_2 is the volume fraction of material 2, ρ_1 is the density of material 1, and ρ_2 is the density of material 2.

Both Richardson [19] and Urick [20] have shown Wood's effective medium model to be an accurate method of obtaining mixture component moduli from measured effective sound speeds. Richardson used Wood's Equation to obtain the bulk moduli of sand grains. Urick used Wood's effective medium model to determine the bulk moduli of finely divided particles in a mixture, both of which are directly applicable to this experiment. Urick neglected the effects of scattering, assumed that the density of the mixture could be extracted from the volume fractions, and assumed that the finely divided particles were very small compared to the wavelength of sound. Urick found that having the particles be less than 1/100 of the wavelength provided accurate results [20].

Since the sample in this experiment had been degassed, it was modeled as simply a two-phase medium: seagrass tissue and water.

2.6 Results

The acoustic pressure at a location inside the sample-filled resonator was acquired by the hydrophone for the 50 Hz–15 kHz chirp signal for an initial measurement and subsequent tests made on 5 minute intervals. The amplitude of the pressure is plotted in Figure 2.5, showing the first 2 modes of *T. testidinum* and the first 4 modes of *H. wrightii*, with the exception of only 3 modes being visible during the intial measurement. By taking the resonance frequencies where pressure maximums occur and converting them into sound speeds using the methods described in Section 2.5.1, then applying the elastic waveguide correction, as described in Section 2.5.2, Figures 2.6 and 2.7 show the free field phase speed versus frequency for the seagrass and water mixtures.

2.6.1 Modes and Sound Speeds

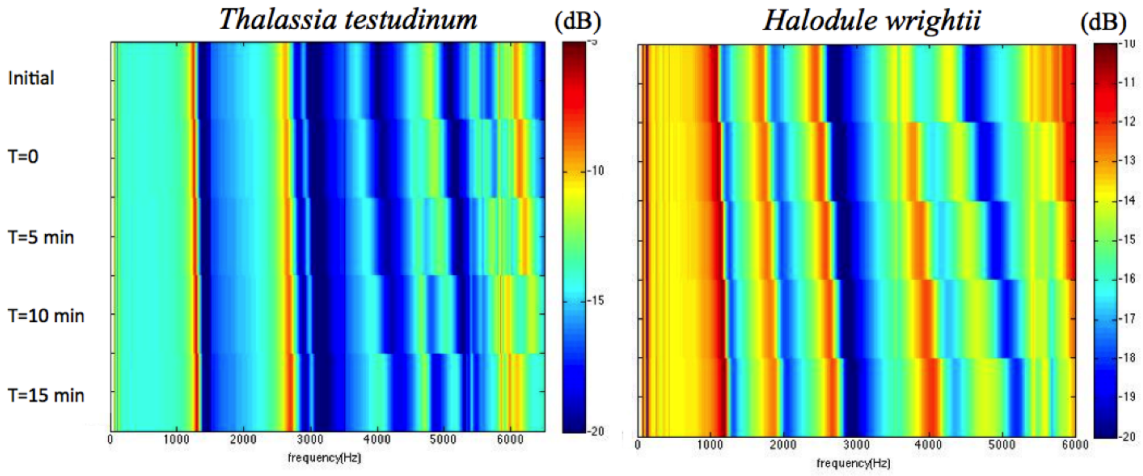

Figure 2.5: Amplitude of pressure response for mode visualization.

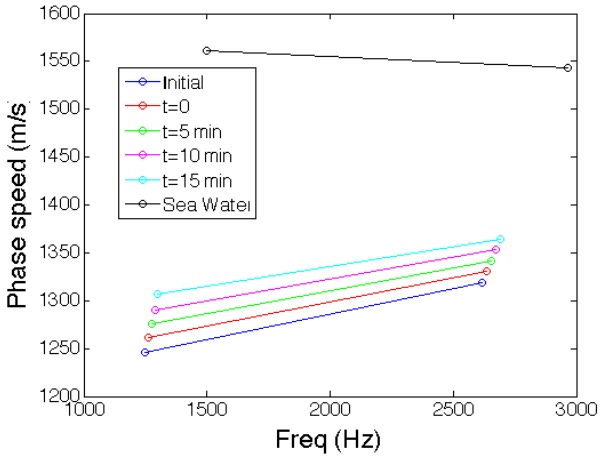

Figure 2.6: Free field phase speed of *Thalassia testudinum* at 27.5 ° C.

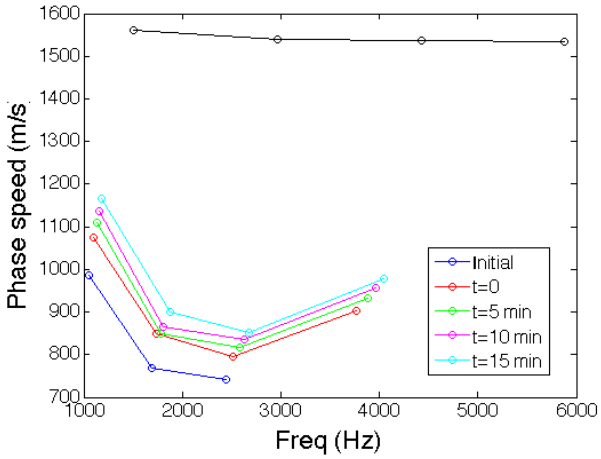

Figure 2.7: Free field phase speed of *Halodule wrightii* at 23.5 ° C.

2.6.2 Obtaining the Bulk Modulus

From the free field sound speed calculated by correcting for the elastic waveguide effect, and measurements of the effective density given by Equation 2.4, the effective bulk modulus was calculated through use of Equation 2.5. It should be noted that the effective free field sound speed used to calculate the bulk modulus was simply an average of the sound speeds shown in Figures 2.6 and 2.7. In other words, the dispersion and temporal variability visible in the extracted sound speeds was ignored for this work. The averaging was justified because the goal of these experiments was to obtain a basic understanding of the acoustic behavior of these species of seagrass and future experiments would be able to focus on dispersion and temporal variability. Solutions of Equation 2.3 for the bulk moduli of the seagrass tissues B_{grass} yield Equations 2.4 through 2.7:

$$\rho_{\text{eff}} = \beta_{\text{grass}}\rho_{\text{grass}} + \beta_{\text{water}}\rho_{\text{water}}, \tag{2.4}$$

$$c_{\text{eff}} = \sqrt{\frac{B_{\text{eff}}}{\rho_{\text{eff}}}}, \tag{2.5}$$

$$\frac{1}{B_{\text{eff}}} = \beta_{\text{grass}}B_{\text{grass}} + \beta_{\text{water}}B_{\text{water}}, \tag{2.6}$$

$$B_{\text{grass}} = \frac{\beta_{\text{grass}}}{\frac{1}{(\beta_{\text{grass}}\rho_{\text{grass}}+\beta_{\text{water}}\rho_{\text{water}})c_{\text{eff}}^2} - \frac{\beta_{\text{water}}}{\rho_{\text{water}}c_{\text{water}}^2}}, \tag{2.7}$$

as functions of the temporally averaged, spectrally averaged, and elastic-waveguide-corrected experimental sound speeds c_{eff}, and the measured seagrass tissue and water densities. The resulting tissue bulk moduli, along with all the input parameters, are shown in Table 2.1.

	c_{eff}(m/s)	ρ_{eff}(kg/m^3)	β_{grass}	β_{water}	B_{water}(Pa)	B_{grass}(Pa)
T. testudinum	1309	908	0.482	0.518	2.47×10^9	1.11×10^9
H. wrightii	921	965	0.556	0.444	2.46×10^9	5.35×10^8

Table 2.1: Bulk modulus and density results for seagrasses.

2.7 Discussion

The experiment yielded data for sound speeds of the two species in roughly the 1 kHz to 4 kHz range. For *Thalassia testidinum*, two clear resonances were seen (see Fig 2.6), whereas for *Halodule wrightii* (see Fig 2.7), four clear resonances were seen (with the exception of the initial measurement taken in which only three resonances were visible). A water-filled tube showed more resonances than the seagrass-water samples, illustrating an attenuating effect of seagrass which supports the findings of the earlier research cited in Section 2.1. At low frequencies, sound speed was found to vary with frequency, illustrating that there is clear dispersion in sound travelling through these species of seagrass. At this time, the dispersion remains unexplained and is the subject of future work.

As time increased, the sound speed tended to steadily increase. At first, temperature was investigated as a potential cause of this effect. However,

since the variation in temperature that would have been seen (cooling down) would have resulted in a steadily decreasing sound speed, temperature does not seem to be the cause. Furthermore, the temperature range in this experiment (6.5 ° C) simply would not result in the scale of sound speed variation that was witnessed.

The next hypothesis was that over time the homogenous mixture gradually began to develop a density gradient. Though the overall density of the mixture would have remained the same, the top of the sample would have shifted to a lower density whereas the bottom of the sample would be of a higher density. This hypothesis was tested with a finite element model in COMSOL in which the three resonance modes were compared between two cases (shown in Fig 2.8). The first case consisted of a sample with a consistent density of 908 kg/m^3 and sound speed of 1307.8 m/s, aligning with the findings for *T. testidinum*. The second case consisted of sample with a 9.5 % difference in density between the top and bottom, which was developed over 10 separate layers. The average density for this case was still 908 kg/m^3. The sound speeds of the layers were calculated with Wood's Equation using the bulk moduli and density for *T. testidinum* and seawater yielded from the experiment. For each case, the tube had a pressure release top and bottom with rigid side walls.

The COMSOL model yielded resonance peaks at 1527, 3054, and 4581 Hz for the constant density case, resulting in a sound speed of 1393.8 m/s for the first three resonances of the sample inside the tube. In the density gradient

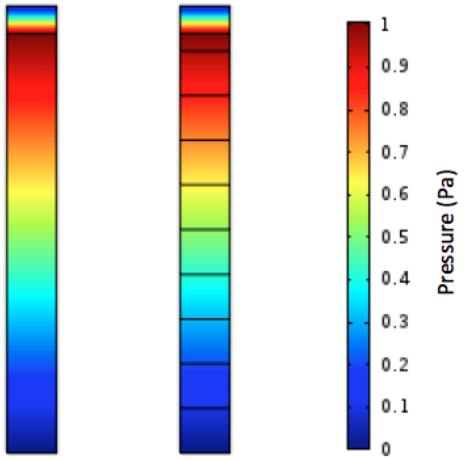

Figure 2.8: Response of COMSOL model to 1 Pa pressure wave at frequency of 107 Hz with a constant density sample, left, and a sample with a density gradient, right.

case, the resonances were at 1532, 3067, and 4601 Hz, resulting in an average sound speed of 1399.4 m/s for these resonances. Although the COMSOL model predicted the correct pattern of the sound speed shifting upwards with an increased density gradient, the amount of this effect is only about 6 m/s, whereas in the experiments the sound speed increased by over 50 m/s with a density gradient of likely less than 9.5 %. Therefore, it is hypothesized that this increase in sound speed with time is caused by the properties of the tissue in the mixture changing with time.

The low-frequency bulk modulus calculated for *Thalassia testidinum* was 1.11×10^9 Pa whereas for *Halodule wrightii* it was 5.35×10^8 Pa. The author is aware of only one previous report of directly measured seagrass tissue bulk moduli: Randall and Hermand's 2013 experiment with *Ecklonia radiata*

[21]. Two methods were used in [21] to determine sound speed of the blades: travel time measurements with a known mixture of finely blended macroalgae and a pulse and echo method with stacks of blades. It should be noted that the success of the finely divided *Thalassia testidinum* and *Halodule wrightii* experiments was highly influential to its use in Randall and Hermand's measurement of the sound speed in *Ecklonia radiata*. Randall and Hermand's experiment yielded a bulk modulus of 3.11×10^9 Pa for the blade-stacking method and 3.10×10^9 Pa for the "soup" method. These values are slightly higher than the values found for *Thalassia testidinum* and *Halodule wrightii*, but since they are different species they seem reasonable.

An expected bulk moduli of *Thalassia testidinum* can found from published values of the elastic moduli, E, and the Poisson ratio, ν. *T. testidinum* has had a range of reported values [22] from 4×10^8 Pa to 2.4×10^9 Pa. Though no direct reporting of the Poisson ratio was found, a Poisson ratio was found to be $\nu = 0.3$ for terrestrial plant leaf parenchyma [23]. Using Equation 2.8:

$$B = \frac{\frac{E}{3}}{1 - 2\nu}, \tag{2.8}$$

the expected bulk moduli, B, ranges between 3×10^8 Pa and 2×10^9 Pa, bracketing the values determined in this work.

Since the bulk modulus of the seagrass was found during this experiment, and the structure of the two species has already been modeled using computed tomography [13], the shear modulus is all that is needed to complete

the model of propogation in these two species of seagrass. The shear modulus could be calculated by taking shear wave measurements of the mixture in the resonance tube, however, this method would yield the shear modulus of the tissue and water mixture and would need to be manipulated to obtain the shear modulus of the seagrass tissue itself. On the other hand, there are common direct shear modulus testing methods which include torsional tests, three-point bending tests, and five-point bending tests [24]. Shear measurements are beyond the scope of the present work and are the subject of future work.

Chapter 3

Properties of Encapsulated Bubbles for Underwater Noise Abatement

3.1 Background and Motivation

Anthropogenic noise sources have the potential to be disruptive and even harmful to marine life and thus there exists a desire to decrease these levels. Noises produced by humans may have such deleterious effects as interfering with the communication and behavior of marine animals, causing animal hearing reduction, and disrupting the echolocation that whales use in order to detect objects [25]. Examples of such anthropogenic noise sources include ship noise, oil and gas exploration and production, and pile driving. The majority of the acoustic noise from these sources is within the 10 Hz to 1 kHz range [25, 26]. As an example of the impacts of noise, a 1991 study found that strong behavioral changes among bowhead whales were seen when broadband noise from 50–1000 Hz was received above levels of 124 dB re 1 μPa [27]. For reference, a 1000 kJ pile driving hammer can typically have a source level of 237 dB re 1 μPa at 1 m with a bandwidth of 100–1000 Hz [28]. Assuming spherical spreading, this piledriving noise could exceed this behavior-related receive level up to 447 km from the source.

One strategy to reduce these anthropogenic noise levels involves using air bubbles. The acoustic effects of bubbles in water, from changing the sound speed, to providing acoustic damping are well-documented and have been the subject of more than a century of research [18, 29]. Starting as early as the 1940's, bubble curtains began being employed as acoustic screens for underwater noise [30]. Traditionally bubble curtains used free bubbles and took advantage of the impedance contrast between air and water, but were significantly less effective at frequencies below 1000 Hz and below 400 Hz extremely ineffective [31–33].

Rather than using traditional free bubble methods, the research being presented here is based upon exploiting the attenuative effects near the resonance frequency of an encapsulated bubble. As for free bubbles, modeling and measurements have both shown that high attenuation and dispersion can be found near the resonance frequency of an encapsulated bubble [34]. This desired attenuation is due to three damping mechanisms: thermal damping, viscous damping, acoustic radiation damping [34]. Compared to a free bubble, an encapsulated bubble allows for larger sized bubbles that can be matched to a desired resonance frequency. A large free bubble, on the other hand, cannot be guaranteed to be the same desired size every time it is produced due to the unstable nature of large free bubbles, as they become increasingly unstable the larger they grow, and have the tendency to break up from their initial spherical cap shape [35]. Furthermore, an encapsulated bubble may be placed in an exact location and does not constantly have to be regenerated,

as freely-rising bubbles do.

3.2 Previous Research of Encapsulated Bubbles for Underwater Noise Mitigation

At the University of Texas, both laboratory resonance tank and free-field attenuation methods with encapsulated bubbles have been performed in order to design an optimal underwater noise mitigation system [36–39]. Laboratory tests were performed in a closed, steel water-filled tank in order to determine the resonance frequency and quality factors of butyl rubber and latex balloons. Both the balloon radii and fill material were varied to determine the response in the tank, which would be used to extrapolate the response in a free-field attenuation measurement. Results showed a trend that followed models [34, 40] of increasing bubble resonance frequency with a decreasing bubble radius [37]. Additionally, attenuation measurements were performed at Lake Travis Test Station (LTTS) using rubber-shelled air-filled encapsulated bubbles [38]. Bubbles of three different sizes were attached to netting on a 2.1 m by 3.7 m steel frame, which enclosed an underwater acoustic source. This experiment found the attenuation to be in close agreement with Church's encapsulated bubble model [34], and with a void fraction of β=0.021, a peak attenuation was seen of nearly 40 dB/m [38].

At OffNoise-Solutions GmbH in Germany, Karl-Heinz Elmer and others have been using controlled elastic gas-filled balloons, referred to as hydro sound dampers, in order to attenuate noise from pile-driving [41–43]. These bubbles

are deployed on frames and nets around piles and have resonances between 200 Hz and 300 Hz. During tests in a wave flume, a wall of bubbles covered 8–10 % of the cross sectional area. Findings reported that these hydro sound dampeners had a maximum noise reduction at approximately 300 Hz and were capable of greater reduction of the sound exposure level (SEL) than an air bubble curtain consisting of free bubbles [42].

3.3 Goals

Expanding on previous studies described in Section 3.2, the overall goal of these experiments was to determine how manipulating physical properties of encapsulated bubbles affects the free field attenuation. Ultimately, the objective is to optimize the efficacy of arrays of encapsulated bubbles for mitigation of anthropogenic underwater noise. These bubbles would need to both provide high attenuation as well as be able to survive deployment and extended operation in the ocean environment.

Unfortunately, testing the attenuation of bubbles in the open water is both expensive and difficult. These tests, which are performed at LTTS to simulate an open water environment, are difficult to schedule since many projects use the testing space and they require significant time to setup and run, require transportation to the site, are costly to the project's budget, and demand construction of a large bubble array. Therefore, the present goal was to determine if a laboratory resonance tank and a larger laboratory test tank could be used to predict attenuation performance in the free field. These

two tanks require considerably less effort and cost to use, and would vastly accelerate the development of the noise mitigation technology. Furthermore, if found that these two tanks could predict free field performance, it was the goal to understand the relation between the laboratory and free field results.

3.4 Overall Experimental Method

The experiments examined the acoustic response of bubbles to a frequency sweep signal at the resonance tank, large outdoor test tank, and LTTS. In each of the test locations, two parameters of the bubbles within the array were varied in order to determine their impact on the response: the bubble wall thickness and bubble fill material. Before running the main tests that examined these two parameters, there were inital tests to determine the bubble diameter and void fraction of the bubbles to use. Tests for the bubble diameter were performed in the lab resonance tank, whereas void fraction was determined with the LTTS tests.

3.5 Resonance Tank Tests

3.5.1 Experimental Setup

The experiments were performed in a closed, cylindrical steel tank filled with water. The tank had an inner radius of 0.5 m, a height of 1 m, and a wall thickness of 1.27 cm. Both the bottom of the tank and the lid placed on the top of the tank were made of steel and were 2.54 cm thick and 5.08 cm thick, respectively. The tank, as shown in Figures 3.1 and 3.2, was completely sealed

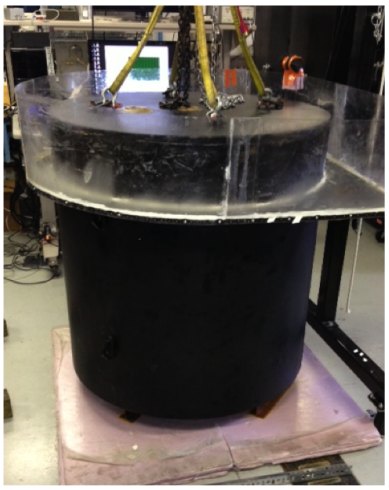

Figure 3.1: Resonance tank with lid attached.

except for two holes on top: one to allow the stinger from the shaker resting on top the tank to penetrate into the water and acoustically excite the tank, and another to allow water to escape from the tank when the lid was placed on the tank. Water in the tank was filtered and then degassed using a conventional pinhole degassing technique [44]. Pseudorandom noise with a frequency range of 10 Hz to 500 Hz was generated by an Agilent 89410A vector signal analyzer (VSA) and then passed through an ElectroVoice Q66 power amplifier before reaching the electromechanical shaker, a Labworks ET-126HF model with a stainless steel circular piston attached.

A Reson TC4013 hydrophone was mounted on the side wall in order to measure the pressure field inside of the tank. The signal from the hydrophone was passed through a Reson CCA1000 hydrophone preamplifier before returning to the vector signal analyzer, where the data was finally acquired.

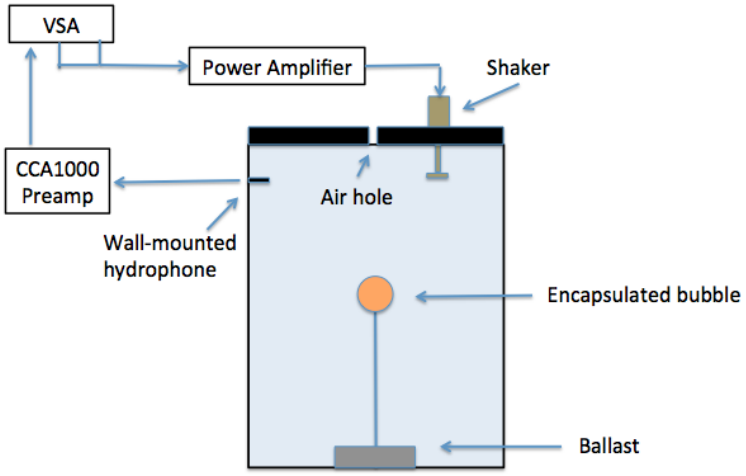

Figure 3.2: Diagram of water-filled resonance tank setup.

The encapsulated bubble was placed in the tank and tied down with a nylon monofilament line to a cylindrical stainless steel ballast. The bubble itself was placed in the center of the tank, thereby being at least several bubble radii from the tank wall in order to give proper mass loading (in other words, mass loading was minimally impacted by the tank walls). The experiments were designed and performed so that water in the tank could behave as a lumped element and were operated in the relatively flat region of the tank response pressure spectrum below the first tank resonance.

3.5.2 Details of Encapsulated Bubbles

The encapsulated bubbles used were Sigma Aldrich 10 mil wall-thickness natural latex rubber laboratory-grade balloons. The air-filled balloon radii were measured by the method of submersion in water and the radii were extracted from the displaced volume. Although the balloons appeared nearly

perfectly spherical, a slight departure from a spherical shape was of little concern since the resonance properties would be negligably impacted [45, 46]. Once at the correct radii, balloons were sealed with nylon cable ties. Six different types of bubbles were tested inside the resonance tank: air-filled single-wall, air-filled double-wall, air-filled triple-wall, helium-filled single-wall, air-filled single-wall with polyester fibers added, and air-filled single-wall with aluminum wool added.

The multiple-walled balloons were tested in order to observe the effect of increasing the shell thickness. Shell thickness is directly related to an encapsulated bubble's durability, where in a final design, a bubble will have to be able to endure multiple deployments and assorted forces from waves and currents. Therefore, knowing the effect of bubble wall thickness on overall attenuation is advantageous. These multiple-walled balloons were created by inserting one uninflated balloon into another uninflated balloon, and then inflating the interior balloon. Once inflated, there was no observed space between balloons, as desired. This method was chosen because there was no other sufficiently practical way to vary the balloon wall thickness directly. It is acknowledged that this method potentially invokes shear forces between the layers of the balloon that differ from what might be found in a thick but homogeneous balloon wall.

Bubble fill material was varied in an attempt to increase the amount of energy lost as heat. Helium has a higher thermal diffusivity than air, and since thermal damping, along with radiation and shell viscous damping were

Figure 3.3: A single walled, 4.68 cm radius balloon filled with 3 g of polyester fibers.

the most effective modes of energy dissipation in the model [34], the goal was to increase the thermal damping, and thus the amount of attenuation provided by the bubbles. The fibrous materials (polyester and aluminum wool) were chosen because they were thermally conductive and could provide extra absorption as heat in the interior of a bubble, similar to how polyester fibers in a speaker increase the overall thermal diffusivity [47]. The polyester added to the bubbles consisted of polyester fibers found in an ordinary pillow. These fibers were weighed and then inserted as small clusters into the balloon before inflation. The inflated polyester balloons are seen in Figure 3.3. The aluminum added to the bubbles was from aluminum wool and was similarly weighed and then added in clusters to the balloons before inflation.

3.5.3 Measurement Technique

A spectral subtraction technique was used to find the resonance frequencies and quality factors of the encapsulated bubbles. This technique has been used to analyze smaller, free bubbles [48, 49] as well as encapsulated bubbles of a similar size [37]. When the tank was acoustically excited by the shaker, the hydrophone pressure measured the total acoustic field in the tank, a summation of the field due to the empty tank and the scattered field of the bubble. Therefore, the scattered field from the bubble can be calculated as:

$$P_{\text{bubble}} = P_{\text{total}} - P_{\text{tank}}. \tag{3.1}$$

In Figure 3.4, the pressure spectra acquired from the empty tank is shown in red, and the total scattered field with the bubble in the tank is in blue. The total scattered field shows three peaks: a bubble resonance, a tank structural resonance, and the first tank mode. Only the bubble resonance peak, however, is of interest for this experiment. The scattered field from the bubble itself is simply the subtraction of the red curve from the blue curve.

The curve in Figure 3.5 demonstrates the scattered field from the bubble itself near the bubble resonance (the results of the subtraction in Eq. 3.1). The specific frequency of maximum pressure amplitude is designated the resonance frequency. In addition to extracting the resonance frequency from the bubble, the quality factor Q is also desired. The quality factor is the bandwidth of the resonance peak at half power divided by the resonance frequency.

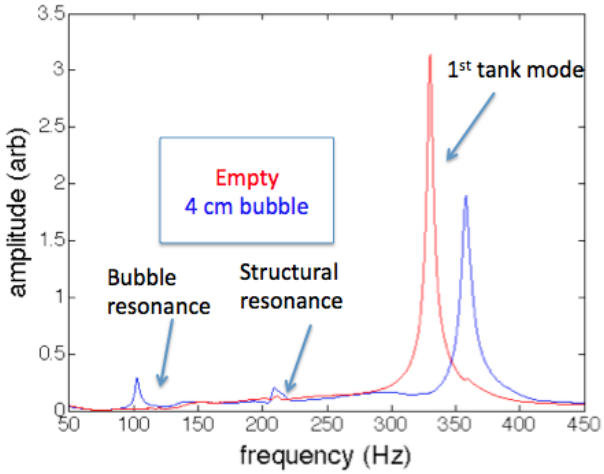

Figure 3.4: Demonstration of the spectral subtraction technique.

The quality factor is also approximately equal to the number of cycles an underdamped oscillator takes to reach steady state and is inversely proportional to the damping coefficient at resonance [37].

Measurements were made in the flat region below the tank resonances in order to avoid effects from reverberation, which are greatest near the tank resonances. However, even near the first tank mode at 350 Hz, previous experimentation with latex shelled bubbles in this resonance tank has shown the resonance frequency to deviate less than 1 % from free-field resonance frequencies [37]

3.5.4 Results

Using the spectral subtraction technique, as described in Section 3.5.3, the resonance frequencies were acquired while the balloon radii and shell thick-

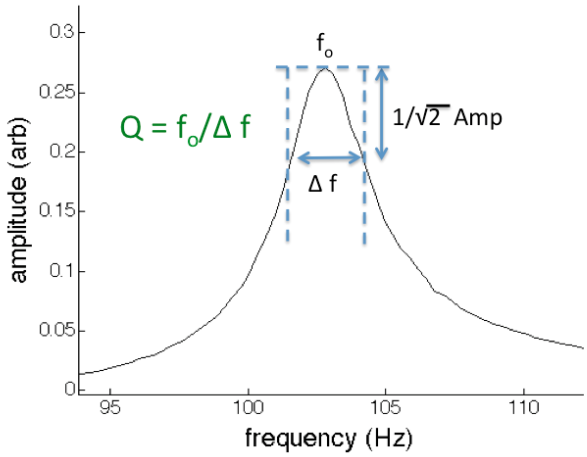

Figure 3.5: The Q factor of the resonance peak.

nesses were varied. Figure 3.6 illustrates these resonance frequencies and demonstrates the trend that increasing the bubble radius decreases the resonance frequency. Furthermore, increasing the wall thickness tends to increase the resonance frequency as well. On average, a double-wall increased the resonance frequency by 3.0 % over a single-wall, whereas a triple-wall increased the resonance frequency by 6.3 % over a single-wall (averaged over the entire measurement range).

Similarly, through the same spectral subtraction technique, the quality factor Q was extracted for the resonances of the multiple-walled balloons (see Figure 3.7). The quality factor Q tended to decrease with increasing balloon radius, but its dependence wall thickness showed a much less consistent pattern. Overall, there was a slight trend for Q to decrease with increasing wall thickness, but there were several examples where the opposite trend was

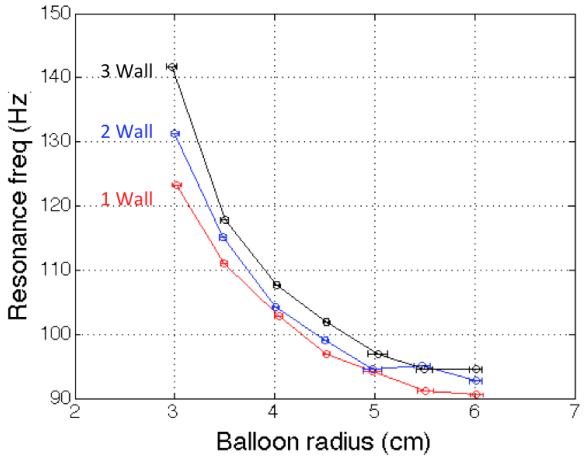

Figure 3.6: Resonance frequency v. bubble radius for multiple-walled balloons.

found, such as when the bubble radius was 5.5 cm. Potentially, at this larger radius, since each wall layer was stretched thinner than it was at smaller radii, the differences between the presence of multiple walls was less pronounced and resonance frequencies were subject to other factors. /clearpage

Balloons with a constant 4.5 cm radii were tested with increased amounts of polyester to determine the effect on the resonance frequency and Q. As shown in Figure 3.8, adding polyester to the bubbles lowered both the resonance frequency and Q. Adding aluminum wool to 4.5 cm radii bubbles did not have as straightforward a pattern, as shown in Figure 3.9. The presence of aluminum wool decreased the resonance frequency, but as more was added, the resonance frequency began to rise. The Q factor dropped with the presence of aluminum wool, but the amount of aluminum wool did not seem to have a significant impact on Q.

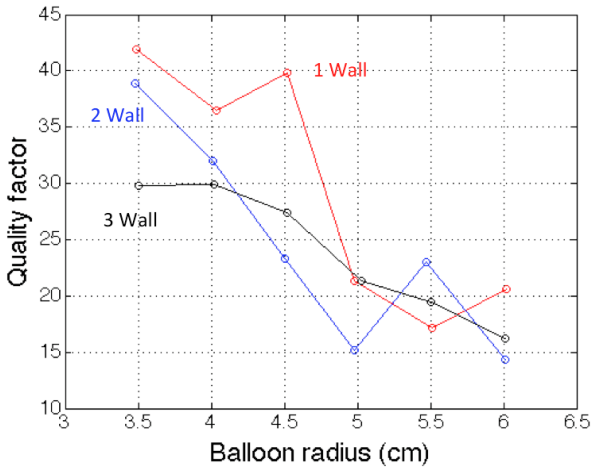

Figure 3.7: Q factor v. bubble radius for multiple-walled balloons.

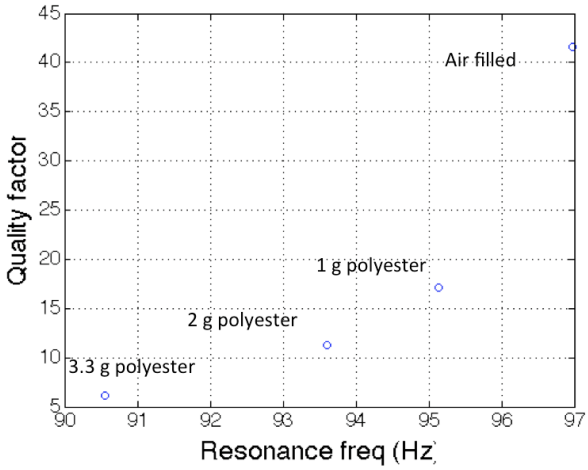

Figure 3.8: Effect on bubble resonance and Q factor of adding polyester to 4.5 cm radius balloons.

Bubbles of 4.68 cm radii were chosen for the LTTS tests due to their convenient resonance just under 100 Hz, their location near the median of all the bubble radii tested, and the ease of their creation based upon available volume displacement tanks in the laboratory. Therefore, further experiments

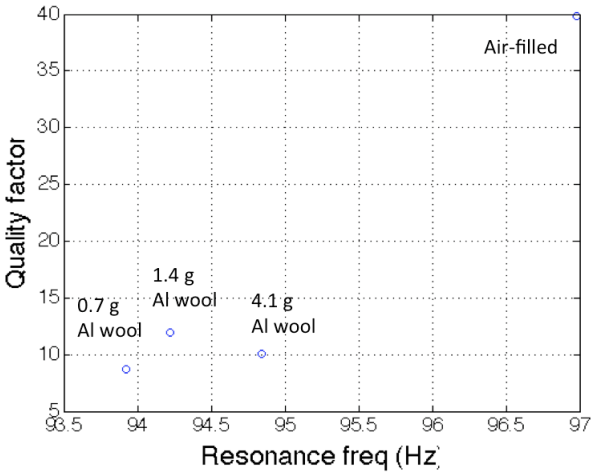

Figure 3.9: Effect on bubble resonance and Q factor of adding aluminum wool to 4.5 cm radius balloons.

were performed in the resonance tank with bubbles with a 4.68 cm radius in order to determine their exact resonance frequencies and Q factors. Figure 3.10 displays the results, in which there are several notable findings. First, the resonance frequencies and Q factors are slightly different than a linear extrapolation between the 4.5 cm and 5 cm bubbles tested earlier. For instance, for an air-filled single-wall balloon, Figure 3.6 would predict a resonance frequency of 96.0 Hz, whereas the test of 4.68 cm balloon demonstated that this value was in fact 92.1 Hz. Secondly, helium was seen to decrease the Q factor and increase the resonance frequency. Finally, the patterns found with the previous tests (reported in Figures 3.6-3.9) were confirmed with these tests. Polyester again showed a decrease in the resonance frequency and Q factor, while adding thickness to the walls increased the resonance frequency.

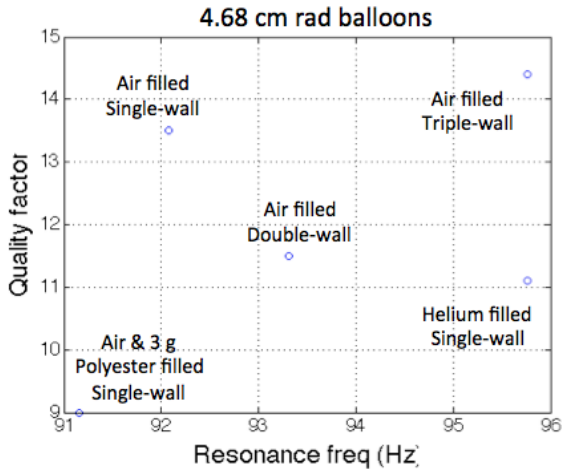

Figure 3.10: Q factor v. resonance frequency for 5 different wall thickness/ fill material combinations for 4.68 cm rad bubbles.

3.6 Outdoor Test Tank and Lake Travis Tests

3.6.1 Experimental Setup

3.6.1.1 General Methods

The apparatus used for the large outdoor test tank and Lake Travis Test Station (LTTS) measurements was nearly identical and it is described for both cases here. A US Navy J-13 compact electromechanical low-frequency acoustic source was suspended in the water from a crane and placed inside of a steel frame. The excitation signal was generated with VIBpoint Framework software on a laptop using a DT9837B Data Translation data acquisition box, amplified by a Crown CE400 power amplifier, and directed to the J-13 which generated a linear chirp from 30 Hz to 2 kHz. The resulting acoustic pressure was then acquired by a HTI-90-U hydrophone at various depths at a distance of 5.23 m away from the sound source in the outdoor test tank and 11.7 m

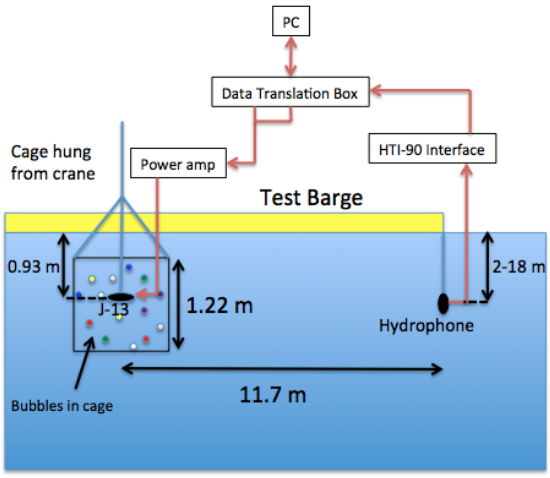

Figure 3.11: Diagram of LTTS testing setup.

away from the sound source at LTTS. The hydrophone signals were band pass filtered from 30 Hz to 2 kHz. A transfer function was measured between the signal acquired by the hydrophone and the signal sent to the J-13 in order to eliminate dependance on the specifics of the electronics used. A transfer function absent of any bubbles was measured and referred to as the reference case. Encapsulated bubbles were then attached to the steel frame and the transfer function was taken again and repeated for each of the cases tested. The dB difference between this transfer function and the reference transfer function illustrates the impact of adding encapsulated bubbles to the system and is referred to in the following pages as noise reduction.

3.6.1.2 Specifics of Outdoor Test Tank Experiments

The large outdoor test tank used in this work is located at Applied Research Laboratories in Austin, Texas. It is constructed of Douglas fir planks

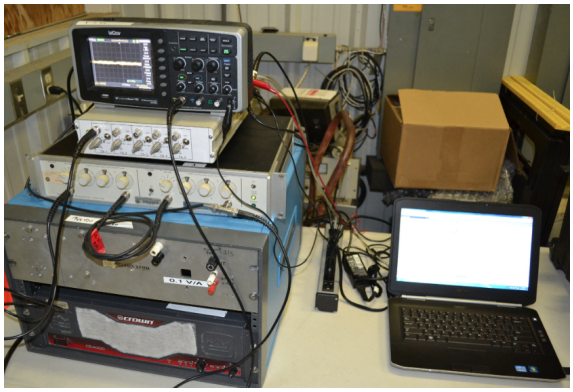

Figure 3.12: Electronics used in experiments. Includes an oscilloscope to visualize signal and a band-pass filter from 30 Hz to 2 kHz.

and has an approximate capacity of 695,000 gallons. The dimensions were 16.76 m in diameter by 11.89 m deep. The acoustic field was measured at a range of depths between 0.5 m and 11.5 m at 1 m increments. The vertical array data was subsequently processed to yield depth-averaged measurements, as discussed in Section 3.6.2.1. The hydrophone was suspended in the water from the deck area, while the supporting electronics were housed in the shed seen in Figure 3.13.

The J-13 was centered axially in the tank and the depth of the J-13 was 0.93 m, measured at the center of the source. The frequency range of the measurements reported here resulted in the excitation of standing waves inside the tank. Further, the excitation signals were continuous in nature, hence the resulting transfer function measurements reported in the following pages represent the steady state reponse of the system. As shown by the transfer function in the reference case, there are clear resonances in the tank

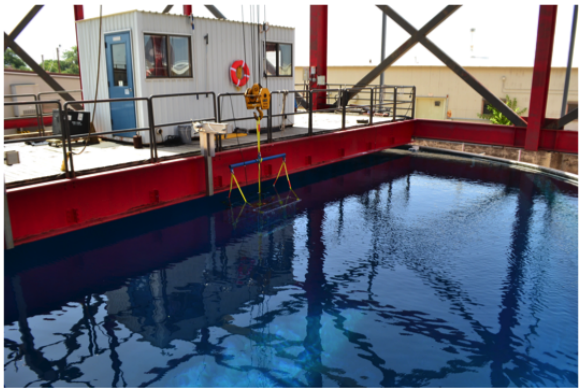

Figure 3.13: Testing in the large outdoor tank.

Figure 3.14: Lake Travis Test Station.

and extracting attenuation from these measurements as if these were free-field measurements is not valid.

3.6.1.3 Specifics of LTTS Tests

The LTTS tests were performed at Lake Travis Test Station near Mansfield Dam in Austin, Texas. Experiments were performed off of the main barge where the water depths were 19.1 m at the source position and 19.6 m at the

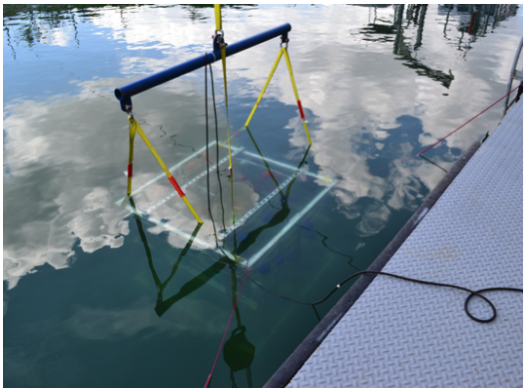

Figure 3.15: Lake Travis Test Station Setup.

hydrophone position. Measurements were taken with the hydrophone at 2 m intervals between depths of 2 m and 18 m. The average transfer function, as presented in Section 3.6.2.2 was a depth-averaged measurement.

The background noise at the lake was significant and had a major impact on the experimental procedures. Background noise measurements were taken at each depth by running a transfer function measurement when the power amplifier was set at zero gain. At certain times of the day, water was released from the dam, causing the background noise to be too high to run the experiments. In addition, there would be various sources of intermittent noise such as motorboats, waves from motorboats, or fish swimming by the hydrophone that required the measurements to be rerun. An oscilloscope was used to determine if these noise sources were present. Transitory noise sources could also be identified through a drop in the coherence of the signal. The coherence of the signal, C_{xy}, which is defined as:

$$C_{\mathrm{xy}} = \frac{|G_{\mathrm{xy}}|^2}{G_{\mathrm{xx}} G_{\mathrm{yy}}}, \tag{3.2}$$

was actively monitored. Here G_{xy} is defined as the cross-spectral density of signals $x(t)$ and $y(t)$ and G_{xx} and G_{yy} are defined as the autospectral densities of $x(t)$ and $y(t)$, respectively. When determining the source level as well as the number of chirps to average over, a high coherence was targeted.

In order to achieve signal over the noise floor in the maximum attenuation band, the source was operated at its maximum power capacity. However, even at maximum power, at void fractions above 0.004 the original setup apparatus could not break the noise floor at the narrow range of frequencies of maximum attenuation. Hence, the maximum void fraction was set sufficiently low, 0.003, so that the maximum attenuation was just higher than the noise floor at that frequency.

3.6.1.4 Details of the Bubble Cage

The bubble cage was constructed out of steel unistrut slotted channels and measured 1.22 m wide by 1.30 m deep by 1.30 m tall. Inner and outer nets, as shown in Figure 3.16, were added to the cage in order to provide a location to attach the bubbles. Bubbles were the same latex balloons used in the resonance tank tests and were attached to the netting with nylon cable ties. All bubbles tested had a 4.68 cm $\pm$ 0.09 cm radius, and following the initial tests where the noise floor obscured the maximum attenuation, tests were performed with 14 bubbles in the cage. Using the volume of the entire

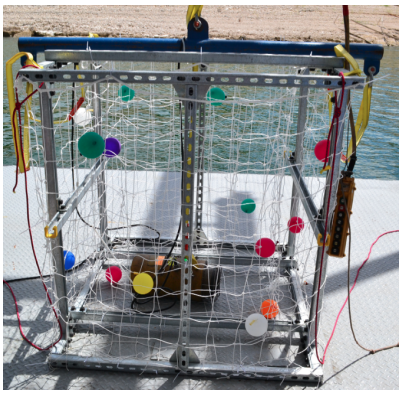

Figure 3.16: The bubble cage.

cage as the total volume, the bubbles provided a void fraction of 0.003. At this void fraction, bubbles were spread out between the inner and outer nets, and were placed on all sides of the cage, surrounding the J-13 acoustic source, but otherwise placed randomly. Five different wall/ fill-material combinations of balloons were tested, which were all in the same configuration in the cage: air-filled single-wall, air-filled double-wall, air-filled triple-wall, helium-filled single-wall, and air-filled single-wall with 3 grams of polyester added. The balloon positions remained constant for each case. The cage was always oriented in the same direction in the water to make sure that the balloon positions relative to the test barge and the receiver also remained constant for each case.

The center of the J-13 was 0.47 m from the top of the cage and 0.93 m from the surface of the water. Both the J-13 and the cage were suspended from a steel support bar (see Figure 3.16) that was attached to an on-site crane.

3.6.2 Results

3.6.2.1 Outdoor Test Tank Results

The tests yielded the hydrophone pressure at 1 m depth intervals in response to the acoustic sweep signal sent through the J-13. Figure 3.17 demonstrates the pressure response obtained at a single depth, as well as the coherence, which was used to determine the reliability of the data and if the noise floor was being approached. The pressures at the individual depths were then averaged to create a depth-averaged response. All proceeding pressures reported will be depth-averaged unless otherwise stated.

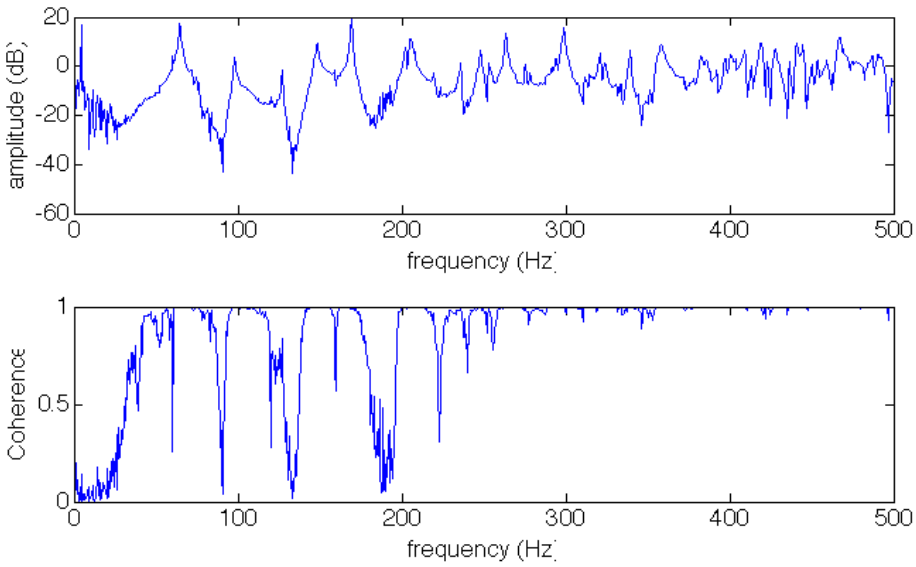

Figure 3.17: Outdoor test tank at pressure at depth of 4.5 m, VF = 0.003, with single-walled air-filled balloons.

The depth-averaged responses of the pressure amplitude in the outdoor test tank are shown in Figure 3.18. The single-wall air-filled balloons demon-

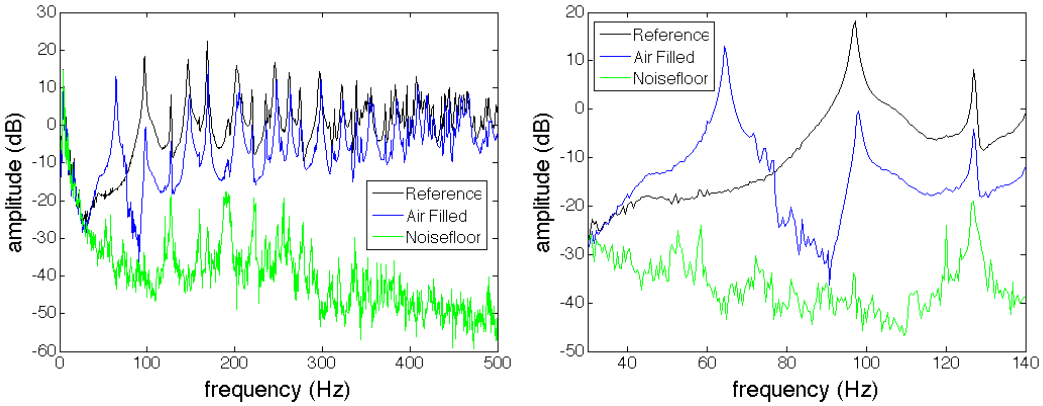

(a) Across sub-500 Hz freq. spectrum (b) Near the individual bubble resonance

Figure 3.18: Outdoor test tank depth-averaged pressure amplitudes of single-walled air-filled bubbles for β=0.003. Includes the noisefloor and reference cases.

strate a clear sound level reduction over the reference case, in which the steel cage had no bubbles attached. The assorted peaks in the reference case exhibit the tank resonances themselves, and convey that the tank response is far from a flat spectrum. The greatest noise reduction is seen at 90.8 Hz, which is very close to the resonance observed in Section 3.5.4. It should be noted that at 64.5 Hz there is an amplification of the signal.

Tests were also performed with a higher void fraction of β=0.01. Figure 3.19 displays the results of these tests, demonstrating an overall higher noise reduction in air-filled bubbles than the β=0.003 tests. Bubbles with 3 grams of polyester added tend to generaly perform quite similarly to the air-filled bubbles; however, air-filled bubbles provide a higher peak noise reduction. It should be noted that with a higher void fraction, the frequency of the sub-

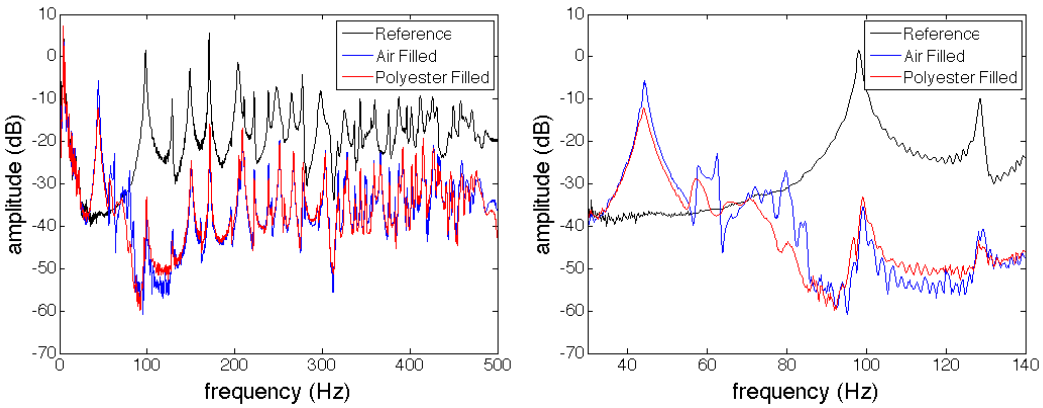

(a) Across sub-500 Hz freq. spectrum (b) Near the individual bubble resonances

Figure 3.19: Outdoor test tank depth-averaged pressures amplitudes of single-walled air-filled and single-walled air and 3 g polyester-filled bubbles for β=0.01. Includes the noisefloor and reference cases.

resonance signal amplification in air-filled bubbles is lowered.

3.6.2.2 LTTS Results

After averaging the pressure responses over the 9 measured depths, the depth-averaged results are shown in Figure 3.20 for an array of bubbles with varying wall thickness with a void fraction of β=0.003 at LTTS. Except for the frequencies close to the bubble resonances where there is the most noise reduction, the noise floor is much lower than the received signal. When focused in near the bubble resonance, adding a thicker shell tended to increase the frequency of maximum noise reduction but decrease the amplitude of maximum noise reduction.

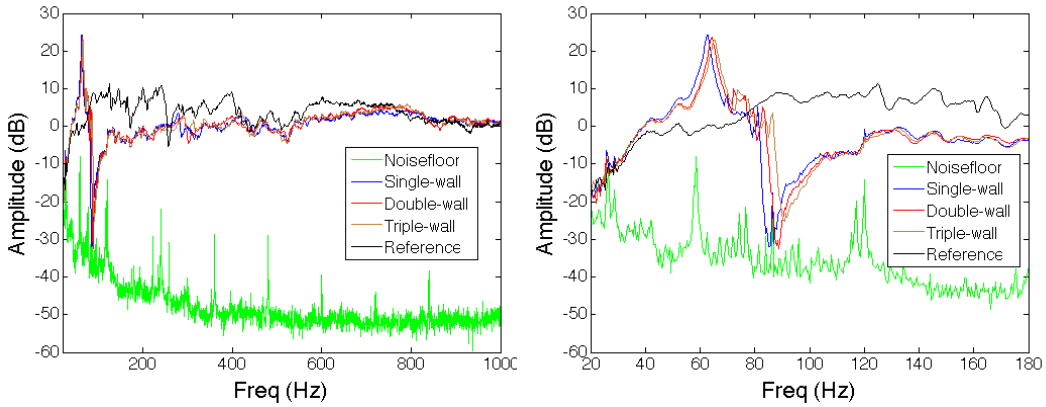

(a) Across sub-500 Hz freq. spectrum (b) Near the individual bubble resonances

Figure 3.20: LTTS depth-averaged pressure amplitudes while varying the wall thickness for β=0.003. Includes single-wall, double-wall, and triple-wall bubbles as well as the noisefloor and reference cases.

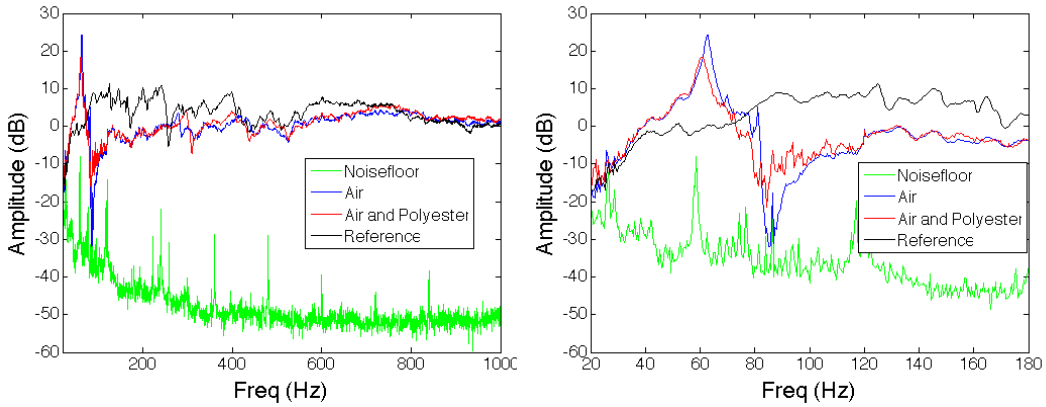

(a) Across sub-1 kHz freq. spectrum (b) Near the individual bubble resonances

Figure 3.21: LTTS depth-averaged pressure amplitudes while varying fill material for β=0.003. Includes single-wall air-filled and single-wall air + 3 g polyester-filled bubbles as well as the noisefloor and reference cases.

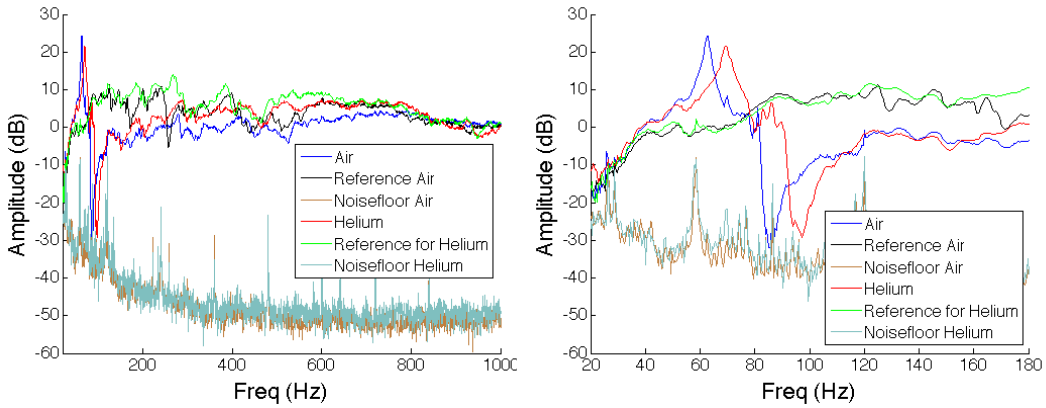

(a) Across sub-1 kHz freq. spectrum (b) Near the individual bubble resonances

Figure 3.22: LTTS depth-averaged pressure amplitudes while varying interior gas for β=0.003. Includes single-wall air-filled and single-wall helium-filled bubbles as well as the noisefloor and reference cases.

Similarly, Figures 3.21-3.22 demonstrate the depth averaged pressure amplitudes against frequency for bubbles with 3 grams of polyester added as well as helium filled bubbles. The helium tests were performed on a different day from the rest of the tests at LTTS and therefore there are minor differences in the reference and noisefloor spectra between days.

The initial tests at LTTS were performed with higher void fractions, but unfortunately the noise floor prevented observation of the exact amount of noise reduction near the bubble resonances. Data from these tests, shown in Figure 3.23, nevertheless convey the increased noise reduction provided by the increased void fractions at frequencies above 100 Hz. However, at frequencies above 1000 Hz, the pattern of increased attenuation with increased void fraction starts to become less valid.

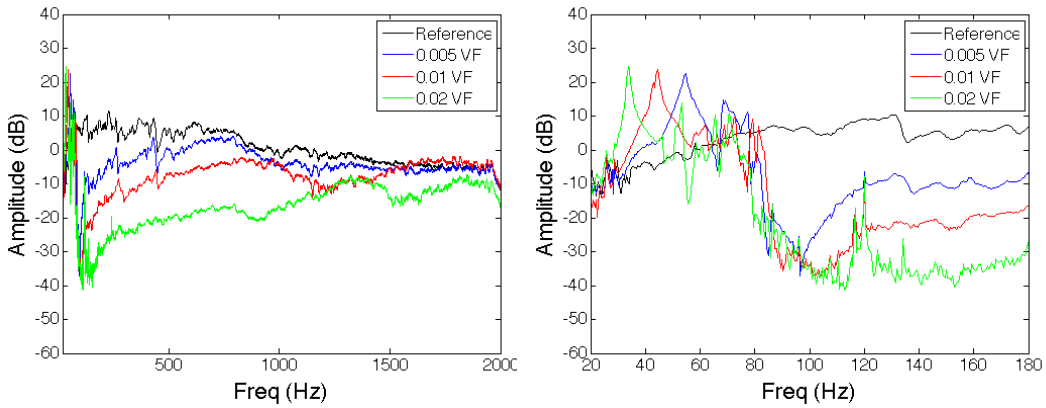

(a) Across sub-2 kHz freq. spectrum (b) Near the individual bubble resonance

Figure 3.23: LTTS depth-averaged pressure amplitudes of single-wall air-filled bubbles while varying the void fraction. Includes β=0.005, 0.01, and 0.02 as well as the reference case.

3.6.3 Analysis

By subtracting the pressure response of the particular bubble configurations from the reference case, it is possible to determine the noise reduction provided by the bubbles. Figures 3.24-3.25 show the noise reduction by the different types of bubbles both through broad frequency ranges as well as close to the bubble resonances.

As shown in the Figure 3.24, there is significant noise reduction for single-wall bubbles in the outdoor test tank when β=0.003 from approximately 78 Hz to 99 Hz. When β= 0.01, there is significant noise reduction at that frequency range, however, at frequencies above 99 Hz, noise reduction still remains significant and does not have the extreme dropoff that is witnessed

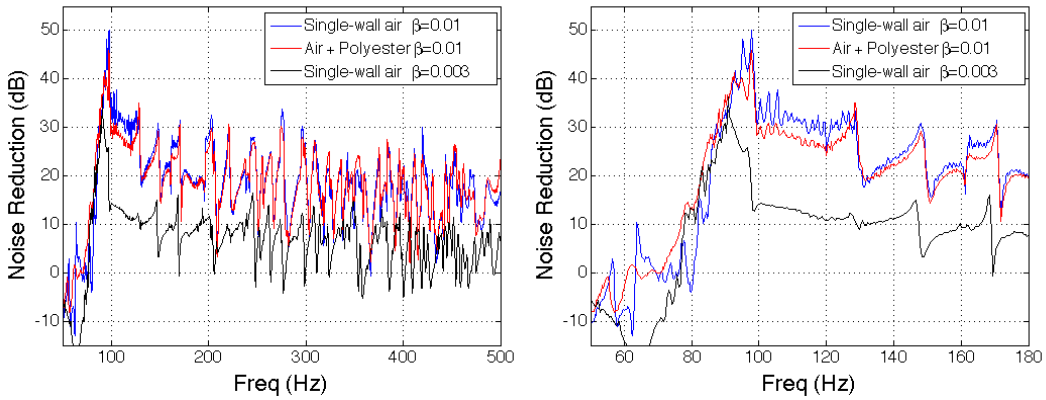

(a) Across sub-500 Hz freq. spectrum (b) Near the individual bubble resonances

Figure 3.24: Noise Reduction in the outdoor test tank for single-wall air-filled bubbles at β=0.01, single-wall air + 3 g polyester-filled bubbles at β=0.01, and single-wall air-filled bubbles at β=0.003.

at β=0.003. Furthermore, the increased void fraction provides a 7 Hz higher frequency of maximum noise reduction for the single-wall air-filled bubbles. Bubbles with polyester added provide overall less noise reduction, however, at frequencies of under approximately 90 Hz, the polyester balloons tend to perform better.

With the LTTS tests, single and double-wall bubbles had the greatest maximum attenuation (see Fig 3.25). As the wall thickness increased, the frequency of maximum attenuation tended to increase. The helium, polyester-filled, and triple-wall bubbles had less maximum noise reduction than the single and double-wall air-filled bubbles. Though the helium bubbles' peak noise reduction was less, between 100-300 Hz they outperformed all other tested bubbles.

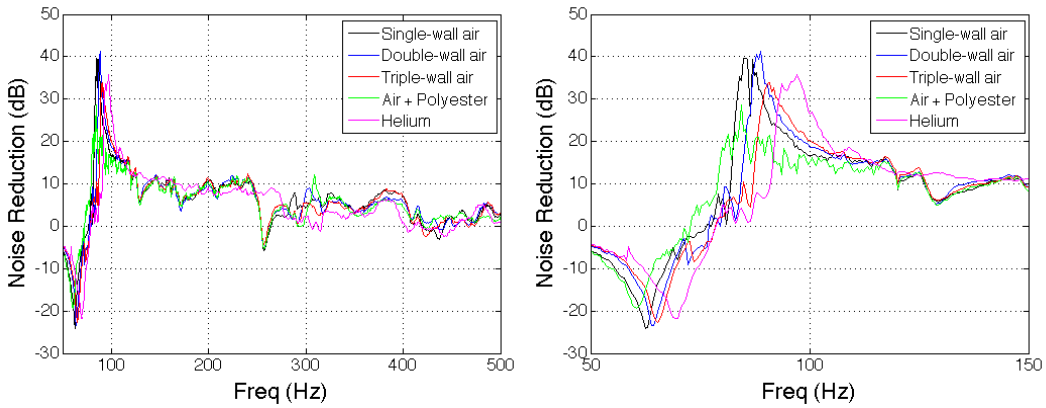

(a) Across sub-500 Hz freq. spectrum (b) Near the individual bubble resonances

Figure 3.25: Noise Reduction with β=0.003 at LTTS. Includes all five bubble wall thickness/ fill material combinations.

The signal amplification seen below the bubble resonance had a strong dependence on the frequency of maximum attenuation at LTTS, as shown in Figure 3.26. On average the peak of the signal amplification was at 72% of the frequency of the maximum noise reduction. One hypothesis is that the amplification is due to a cloud resonance of the entire array of bubbles in the cage. Since the peak of this amplification tended to decrease with increased void fraction (see Figure 3.23), this hypothesis seems even more likely. For a more detailed investigation of amplification being caused by a cloud resonance, see the 2014 Ph.D. dissertation of Craig Dolder [50].

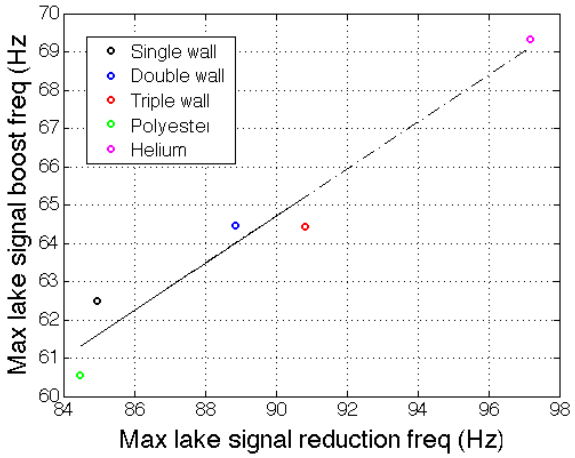

Figure 3.26: Comparison between the frequency of maximum attenuation in LTTS tests for β =0.003 to frequency of maximum signal amplification. Includes all five bubble wall thickness/ fill material combinations

3.7 Comparison of Lab Resonance Tank, Outdoor Test Tank, and LTTS Tests

Since bubbles in the resonance tank were only at a depth of 0.5 m, as opposed to a 1.12 m depth on average in the outdoor test tank and LTTS, a conversion was necessary for proper comparison. By inspecting the Minnaert bubble resonance model:

$$f = \frac{1}{2\pi a}\sqrt{\frac{3\nu p_{\mathrm{A}}}{\rho}}, \tag{3.3}$$

where f is the resonance frequency, ν is the polytropic coefficient, a is the bubble radius, ρ is the density of the liquid surrounding the bubble, and p_{A} is the ambient pressure, it becomes apparent that the square root of the ratio of the ambient pressures is all that is needed to convert between the two depths. Once this conversion was applied, the frequency of the maximum noise

reduction could be compared to the laboratory resonance tank resonance frequencies. For single-wall air-filled bubbles, the maximum noise reduction at β=0.003 was at 84.9 Hz at LTTS, 90.8 Hz at the outdoor test tank, while the depth-adjusted resonance frequency in the laboratory tank was 94.6 Hz. A comparison was further made between the frequency of maximum noise reduction of the five bubble types tested at LTTS and their resonance frequencies in the laboratory tank. As shown in Fig 3.27, there is a strong positive correlation between the depth-adjusted resonance frequency and the frequency of maximum noise reduction at LTTS. However, it should be noted that these two frequencies are not the same; the tank resonance frequencies were consistently higher than the LTTS max noise reduction frequencies at β=0.003.

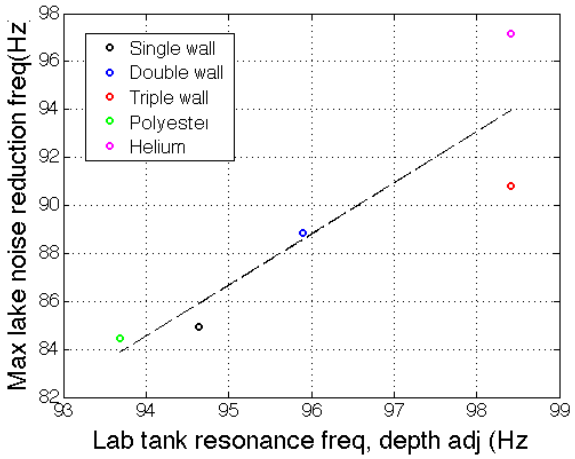

Figure 3.27: Comparison between the frequency of maximum noise reduction in LTTS tests for β =0.003 to resonance frequency in the lab resonance tank, depth adjusted. Includes all five bubble wall thickness/ fill material combinations.

Overall, frequencies of maximum noise reduction were highly correlated

to the values of the resonance frequency, but varied depending on which body of water they were tested in (LTTS or the outdoor test tank), as well as the void fraction in which the tests were performed. Typically a higher void fraction resulted in a higher frequency of maximum attenuation. If the void fraction was high enough, the frequency of maximum attenuation could even be higher than the laboratory tank resonance frequency. The scenario of the air-filled single-wall and polyester bubbles in the outdoor test tank with β=0.01, as shown in Figure 3.24 provides this condition.

The Q factor was compared to the amplitude of the max noise reduction at LTTS and is shown in Figure 3.28. There is a general trend that a higher Q factor results in a higher peak noise reduction. This trend is expected from Church's model [34] as more bubble wall motion results in more attenuation. When comparing a more broadband frequency range around the bubble resonance, rather than at a single frequency, this pattern of a higher Q factor being correlated with more noise reduction appears again and even more prominently. Figure 3.29 illustrates this principle with a frequency range of 75-120 Hz, a range chosen because of its ability to encompass all of the greatest attenuation peaks near bubble resonance.

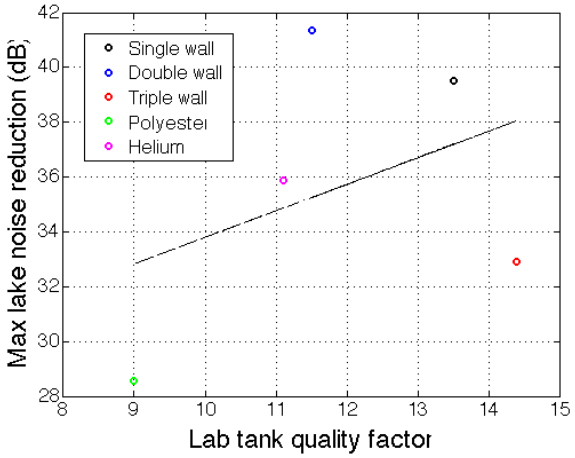

Figure 3.28: Comparison between the amplitude of maximum noise reduction in LTTS tests for β =0.003 to Q factor in the lab resonance tank. Includes all five bubble wall thickness/ fill material combinations.

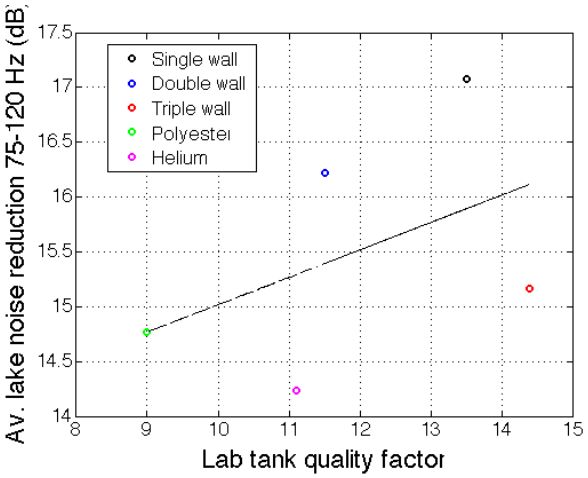

Figure 3.29: Comparison between the average amplitude of noise reduction from 75-120 Hz in LTTS tests for β =0.003 to Q factor in the lab resonance tank. Includes all five bubble wall thickness/ fill material combinations.

As illustrated in Figures 3.27–3.29, air-filled single-wall balloons and air-filled double-wall balloons tended to have the greatest maximum noise reduction. Although double-wall had the greatest reduction at a single frequency, if taken at a broader range of 75–120 Hz, which in deployment is a more practical metric of performance than at a single frequency, the single-wall air-filled balloons had the greatest noise reduction. Consequently, in real-world use, encapsulated bubbles should have the thinnest possible wall that will permit survival in deployment and extended operation. Moreover, with the fill materials tested, it seems that air-filled bubbles are still the best option. Finally, with the correlations shown in Figures 3.27–3.29, it is clear that it is in fact possible to relate the response of a single encapsualted bubble in a small laboratory tank to the noise reduction of an array of encapsulated bubbles in open water tests.

Chapter 4

Conclusion

Motivations, methods, and results have been described for experiments with two categories of multiphase materials: seagrass and encapsulated bubbles. These experiments yielded results that may be used for future propagation and attenuation models. In addition, the report examined the experimental methods themselves and observations were made on the procedures' effects on the data.

With seagrass, an experiment was performed in order to determine the low frequency compressibility of *T. testidinum* and *H. wrightii* tissue. By using mixtures of finely divided tissue and seawater in a glass resonator tube, and applying chirps from a LDS V10 L shaker, the effective sound speeds of the mixtures were extracted at the specific resonance frequencies. Due to the attenuative nature of the seagrass tissues, only 2–4 resonances were visible in the tube. The seagrasses had unexpected and so-far unexplained dispersion, and some temporal variability and so the effective sound speeds were averaged over the resonance frequencies as well as over time. Then, after applying the elastic waveguide equation and Wood's equation, the bulk moduli were extracted for the seagrass species. Through further analysis, as well as a COMSOL finite

element model, it was hypothesized that the sound speed's temporal variability was likely due to the material properties themselves shifting during the experimental window. Nevertheless, it is suggested that further experiments be undertaken with this finely divided tissue methodology in order to better understand the nature of these changes. No previously reported values of the bulk moduli were found in the species reported here, but the present measurement of *T. testidinum* of $B = 1.11 \times 10^9$ Pa is bracketed within the extrapolated values from literature of 3×10^8 Pa – 2×10^9 Pa. With these bulk moduli values, as well as knowledge of the tissue structure obtained in previous research [13], only the shear modulus remains to be determined in order to complete the propagation model in these two species of seagrass.

Experiments were performed on encapsulated bubbles in a small laboratory resonance tube, a large outdoor test tank, and at LTTS. These experiments sought to determine the effects of changing the wall thickness and bubble fill material on the resonance frequency and quality factor in the resonance tank and the effects on the noise reduction in the large outdoor tank and LTTS tests. In the resonance tank, the following trends were seen: Increasing the wall thickness increased the resonance frequency. Increasing the wall thickness also decreased the Q factor, but with a less consistent trend. Adding polyester decreased the resonance frequency and decreased the Q factor, whereas helium increased the resonance frequency over air-filled balloons but decreased the Q factor. The addition of aluminum wool created a drop in resonance frequency and Q factor, but as more material was added the

resonance frequency began to rise. The resonance frequencies were relatable to the frequncies of maximum noise reduction in the outdoor test tank and LTTS tests, but the exact relations were dependent on the void fraction and the particular test: a higher void fraction resulted in a higher frequency of maximum attenuation, and the LTTS tests typically had lower frequencies of maximum attenuation than the outdoor test tank experiments for equivalent void fractions. It is hypothesized that the outdoor test tank behaved closer to the laboratory resonance tank because in a way it can be thought of as simply a larger version of the laboratory resonance tank. With the comparitively large dimensions of the tank, the acoustic field does not quite behave fully as a lumped element, the confined space and reflections made it essentially a hybrid field. Additionally, a higher resonance tank Q factor resulted in a generally greater peak noise reduction, consistent with Church's model [34]. With these results it is now possible to test future encapsulated bubbles in either the laboratory tank or outdoor test tank and have a better picture of noise reduction performance in the free field. Furthermore, the data of these experiments may be used to further improve attenuation models.

Appendices

Appendix A

Details of the Elastic Waveguide Equation

$$
\begin{aligned}
1 + [L_{11}(P_m)L_{00}(T_m)]\left(\frac{\pi^2 q_{0m}^2 bdP_m^2 T_m^2}{8E_m^2}\right) + [L_{11}(T_m)L_{00}(P_m)\left(\frac{\pi^2 bdE_m^2}{8q_{0m}^2}\right) \\
+[L_{10}(P_m)L_{01}(T_m) + L_{01}(P_m)L_{10}(T_m)] \times \left(\frac{\pi^2 bdP_m T_m}{8}\right) \\
+[bL_{11}(P_m)L_{10}(T_m) + d(1+Q_m b)L_{11}(P_m)L_{01}(T_m)]\left(\frac{\pi^2 P_m^2 T_m}{8E_m} - \frac{\pi^2 P_m^2 q_{0m}^2 T_m}{8E_m^2}\right) \\
+[bL_{11}(T_m)L_{10}(P_m) + d(1+Q_m b)L_{11}(T_m)L_{01}(P_m)]\left(\frac{\pi^2 P_m E_m}{8q_{0m}^2} - \frac{\pi^2 P_m}{8}\right) \\
+[(1+Q_m b)L_{11}(T_m)L_{11}(P_m)]\left(\frac{\pi^2 P_m^2}{8q_{0m}^2} + \frac{\pi^2 P_m^2 q_{0m}^2}{8E_m^2} - \frac{\pi^2 P_m^2}{4E_m}\right) = 0.
\end{aligned}
\tag{A.1}
$$

The real solutions to the elastic waveguide equation, Eq. A.1, are q_{0m}. This is the wavenumber of the m^{th} mode at that frequency. Here:

$$L_{mn}(y) = J_m(dy)Y_n(by) - J_n(by)Y_m(dy) \tag{A.2}$$

$$P_m = \sqrt{k_c^2 - q_{0m}^2} \tag{A.3}$$

$$T_m = \sqrt{k_s^2 - q_{0m}^2} \tag{A.4}$$

$$k_c = \omega / C_c \tag{A.5}$$

$$k_s = \omega / C_s \tag{A.6}$$

$$Q_m = \frac{\rho_l \omega^2 b J_0(X_{0m})}{2\rho_w C_s^2 X_{0m} J_1(X_{0m})} \tag{A.7}$$

$$E_m = q_{0m}^2 - k_s^2/2 \tag{A.8}$$

List of variables and function types used:

ω=angular frequency

C_c = compressional wavespeed in the solid

C_s = shear wavespeed in the solid

b=inner tube radius

d= outer tube radius

ρ_w = density of tube wall

ρ_l = density of tube liquid

J_n=n^{th} order Bessel function of the first kind

Y_n=n^{th} order Bessel function of the second kind.

Appendix B

Sample MATLAB Scripts

B.1 Glass Resonator Tube

```
load X12101210.ASC
vary=zeros(5,1601);
sig1 = X12101210(1:450,:);
vary(1,:)=X12101210(:,2);
figure(1)
%% Enter length of tube and data file
% Run it once, estimate resonance frequencies, enter them as
% 'approxpeaks', then run again.

L = 0.4564-.016;  %  length of tube filled (m)
L_err = .0014; % possible error in measurement of L (m)
% T = 21.4C

approxpeaks = [1000 1800 2400]; % approx. freq. resonances [Hz]
tolerance = 300; % look for peaks at 'approxpeaks' locations
%plus or minus tolerance [Hz].
```

```
%% plot spectrum

f = sig1(:,1);
P = 20*log10(abs(sig1(:,2)));

figure(1),subplot(2,1,1)
plot(f,P)
xlabel('frequency (Hz)')
ylabel('amplitude (dB)')
title('Halodule Soup')

%% Peak finder

ii = 1;
for nn = 1:length(f)
    for mm = 1:length(approxpeaks)
        if f(nn) > approxpeaks(mm)-tolerance && f(nn) <
approxpeaks(mm)+tolerance
            prange(mm,ii) = P(nn);
            ii = ii+1;
        end
    end
end
```

```
for mm=1:length(approxpeaks)
      peaks(mm,1) = max(nonzeros(prange(mm,:)));
end

for ii = 1:length(f)
    for mm = 1:length(approxpeaks)
        if P(ii) == peaks(mm,1)
            freqs(mm,1) = f(ii);
        end
    end
end

subplot(2,1,1)
hold on
plot(freqs,peaks,'bo')
xlim([min(f) max(f)])

n = 1:length(peaks); % <-- Use this as default.

%%  calculate dispersive sound speed

subplot(2,1,2)
```

```
CC = freqs.*(2*L./[1:max(n)]')
hold on
plot(freqs,CC,'-o')
E= (freqs+3.10945).*(2*(L+L_err)./[1:max(n)]')-CC;
errorbar(freqs,CC,E,'b');
hold on
xlabel('frequency (Hz)')
ylabel('phase speed (m/s)')
```

B.2 Laboratory Resonance Tank

```
load X13042502.ASC
sig1 = X13042502;

figure(1)
approxpeak = 105; % approx. freq. resonances [Hz]
tolerance = 30; % look for peaks at 'approxpeaks' locations
plus or minus tolerance [Hz].

%% plot spectrum
f = sig1(:,1);
P = sig1(:,2);
coherence = sig1(:,3);
phase = sig1(:,4);
```

```
subplot(2,1,1)
plot(f,P)
ylim([-0.5 2]);
xlabel('frequency (Hz)')
ylabel('amplitude (arb)')
title('4cm 1 wall')
set((gca), 'fontsize', 16);
set((gca), 'linewidth',1);

%% Peak finder

ii = 1;
for nn = 1:length(f)
    for mm = 1:length(approxpeak)
        if f(nn) > approxpeak(mm)-tolerance && f(nn) <
approxpeak(mm)+tolerance
            prange(mm,ii) = P(nn);
            ii = ii+1;
        end
    end
end

for mm=1:length(approxpeak)
```

```
      peaks(mm,1) = max(nonzeros(prange(mm,:)));
end

for ii = 1:length(f)
    for mm = 1:length(approxpeak)
        if P(ii) == peaks(mm,1)
            freqs(mm,1) = f(ii);
        end
    end
end

figure(1)
hold on
plot(freqs,peaks,'ro')
xlim([min(f) max(f)])

%% plot coherence

subplot(2,1,2)
plot(f,coherence);
xlabel('frequency (Hz)')
ylabel('coherence')
```

B.3 LTTS Tests

```
load X130822_MidVF_10mc.txt
sig1 = X130822_MidVF_10mc;


%% plot spectrum
figure(1)
f = sig1(:,1);
P = sig1(:,7);
coherence = sig1(:,6);
subplot(2,1,1)
plot(f,20*log10(P))
ylim([-80 20])
xlabel('frequency (Hz)')
ylabel('amplitude (dB)')
title('Single-Walled Balloon 10m 0.02 VF')
subplot(2,1,2)
plot(f,coherence);
xlabel('frequency (Hz)')
ylabel('Coherence')
```

Bibliography

[1] C.N. Dolder and P.S. Wilson. A simple resonator technique for determining the acoustic properties of fish schools. *Journal of the Acoustical Society of America*, 131:3287, 2012.

[2] P.S. Wilson and K.H. Dunton. Laboratory investigation of the acoustic response of seagrass tissue in the frequency band 0.5-2.5 kHz. *Journal of the Acoustical Society of America*, 125:1951–1959, 2009.

[3] J.P. Hermand. *Handbook of Scaling Methods in Aquatic Ecology: Measurement, Analysis, Simulation*. CRC Press, 2004.

[4] A.P. Lyons and D.A. Abraham. Statistical characterization of high-frequency shallow-water seafloor backscatter. *Journal of the Acoustical Society of America*, 106:1307–1315, 1999.

[5] E.M. McCarthy and B. Sabol. Acoustic characterization of submerged aquatic vegetation: Military and environmental applications. *OCEANS 2000 MTS/IEEE Conference and Exhibition*, 3:1957–1961, 2000.

[6] T. Komatsu, C. Igarashi, K. Tatsukawa, S. Sultana, Y. Matsuoka, and S. Harada. Use of multi-beam sonar to map seagrass beds in Otsuchi bay on the Sanriku coast of Japan. *Aquatic Living Resources*, 16:223–230, 2003.

[7] P.J. Mulhearn. Mapping seabed vegetation with sidescan sonar. Technical Report TN-0381, Defense Science and Technology Organization, Australia, 2001.

[8] V. Pasqualini, C. Pergent-Martini, P. Clabaut, and G. Pergent. Mapping of *Posidonia oceanica* using aerial photographs and side scan sonar: application off the island of Corsica (France). *Estaurine, Coastal and Shelf Science*, 47:359–367, 1998.

[9] V.L. Lucieer. Object-oriented classification of sidescan sonar data for mapping benthic marine habitats. *International Journal of Remote Sensing*, 29:905–921, 2008.

[10] J.P. Hermand. Broad-band geoacoustic inversion in shallow water from waveguide impulse response measurements on a single hydrophone: theory and experimental results. *IEEE Journal of Oceanic Engineering*, 24:41–66, January 1999.

[11] D. Chu and P.H. Wiebe. Measurement of sound-speed and density contrasts of zooplankton in antarctic waters. *ICES Journal of Marine Science*, 62:818–831, 2005.

[12] P.S. Wilson and K.H. Dunton. An experimental laboratory investigation of the low-frequency acoustics of seagrasses. *Journal of the Acoustical Society of America*, 119:3448, 2006.

[13] C.J. Wilson, P.S. Wilson, C.A. Greene, and K.H. Dunton. Seagrass leaves in 3-d: Using computed tomography and low-frequency acoustics to investigage the material properties of seagrass tissue. *Journal of Experimental Marine Biology and Ecology*, 395:128–134, 2010.

[14] G. Enenstein, C. Dolder, P.S. Wilson, and J.P. Hermand. Investigation of low-frequency acoustic tissue properties of seagrass. *Proceedings of Meetings on Acoustics*, 19(005007), 2013.

[15] V.A. Del Grosso. Analysis of multimode acoustic propagation in liquid cylinders with realistic bondary conditions– Application to sound speed and absorption measurements. *Acustica*, 24(6):299–311, 1971.

[16] L.D. Lafleur and F.D. Shields. Low-frequency propagation modes in a liquid-filled elastic tube waveguide. *Journal of the Acoustical Society of America*, 97:1435–1445, 1995.

[17] A. Mallock. The damping of sound by frothy liquids. *Proceedings of the Royal Society of London*, 84, 1910.

[18] A.B. Wood. *A Textbook of Sound*. G. Bell and Sons LTD, 1st edition, 1930.

[19] M.D. Richardson, K.L. Williams, K.B. Briggs, and E.I. Thorsos. Dynamic measurement of sediment grain compressibility at atmospheric pressure: acoustic applications. *IEEE Journal of Oceanic Engineering*, 27:593–601, July 2002.

[20] R.J. Urick. A sound velocity method for determinging the compressibility of finely divided substances. *Journal of Applied Physics*, 18:983–987, 1947.

[21] J. Randall, J.P. Hermand, M.E. Arnould, J. Ross, and C. Johnson. Complimentary ultrasound methods for the estimation of sound speed in macroalgae. *Proceedings of Meetings on Acoustics*, 19(005025), 2013.

[22] K. Bradley and C. Houser. Relative velocity of seagrass blades: implications for attenuation in low-energy environments. *Journal of Geophysical Research: Earth Surface*, 114, 2009.

[23] K.J. Niklas. *Plant Biomechanics*. University of Chicago Press, 1992.

[24] S. K. Harrison. Comparison of shear modulus test methods. Master's thesis, Virginia Tech, 2006.

[25] W.J. Richardson, C.R. Greene, C.I. Malme, and D.H. Thomson. *Marine Mammals and Noise*. Academic Press, 1995.

[26] H. Bailey, B. Senior, D. Simmons, J. Rusin, G. Picken, and P.M. Thompson. Assessing underwater noise levels during pile-driving at an offshore windfarm and its potential effects on marine animals. *Marine Pollution Bulletin*, 60:888–897, 2010.

[27] W.J. Richardson, C.R. Greene, W.R. Koski, M.A. Smultea, G. Cameron, C. Holdsworth, G. Miller, T. Woodley, and B. Wursig. Acoustic effects

of oil production activities on bowhead and white whales visible during spring migration near Pt. Barrow Alaska - 1990 phase. Technical Report OCS Study MMS 91-0037, U.S. Minerals Management Services, 1991.

[28] J.A. Hildebrand. Anthropogenic and natural sources of ambient noise in the ocean. *Marine Ecology Progress Series*, 395:5–20, 2009.

[29] T.G. Leighton. *The Acoustic Bubble*. Academic Press, 1994.

[30] D.P. Loye and W.F. Arndt. A sheet of air bubbles as an acoustic screen for underwater noise. *Journal of the Acoustical Society of America*, 20:143–145, 1948.

[31] S.N. Domenico. Acoustic wave propagation in air-bubble curtains in water– Part 1: History and theory. *Geophysics*, 47:345–353, 1982.

[32] B. Wursig, C.R. Greene, and T.A. Jefferson. Development of an air bubble curtain to reduce underwater noise of percussive piling. *Marine Environmental Research*, 49:79–93, 2000.

[33] K. Lucke, P.A. Lepper, M.A. Blanchet, and U. Siebert. The use of an air bubble curtain to reduce the received sound levels for harbor porpoises *phocoena phocoena*. *Journal of the Acoustical Society of America*, 130:3406–3412, 2011.

[34] C.C. Church. The effects of an elastic solid surface layer on the radial pulsations of gas bubbles. *Journal of the Acoustical Society of America*, 97:1510–1521, 1995.

[35] R.M Davies and G.I. Taylor. The mechanics of large bubbles rising through extended liquids and through liquids in tubes. *Proceedings of the Royal Society of London*, 155:375–390, 1950.

[36] K.M. Lee, K.T. Hinojosa, M.S. Wochner, T.F. Argo IV, P.S. Wilson, and R.S. Mercier. Sound propagation in water containing large tethered spherical encapsulated gas bubbles with resonance frequencies in the 50 Hz to 100 Hz range. *Journal of the Acoustical Society of America*, 130:3325–3332, 2011.

[37] K.M. Lee, A.R. McNeese, L.M. Tseng, M.S. Wochner, and P.S. Wilson. Measurements of resonance frequencies and damping of large encapsulated bubbles in a closed, water-filled tank. *Proceedings of Meetings on Acoustics*, 18(075003), 2014.

[38] K.M. Lee and P.S. Wilson. Attenuation of sound in water through collections of very large bubbles with elastic shells. *Proceedings of Meetings on Acoustics*, 19(075048), 2013.

[39] K.M. Lee, P.S. Wilson, and M.S. Wochner. Attenuation of standing waves in a large water tank using arrays of large tethered encapsulated bubbles. *Journal of the Acoustical Society of America*, 135:1700–1708, 2014.

[40] K.W. Commander and A. Prosperetti. Linear pressure waves in bubbly liquids: comparison between theory and experiments. *Journal of the Acoustical Society of America*, 85:732–746, 1989.

[41] K.H. Elmer. Pile driving noise reduction using new hydro sound dampers. European Cetacean Society 2010, March 2010.

[42] K.H. Elmer. Development of a new underwater piling noise mitigation system - using hydro sound dampers (HSD). (OMAE2012-83707), July 2012.

[43] K.H. Elmer. Efficient application of encapsulated bubbles and foam elements to mitigate offshore piling noise. *Journal of the Acoustical Society of America*, 134:4060, 2013.

[44] A.R. Kaiser and C.A. Cain. A cost effective degassing system for use in ultrasonic measurements: The multiple pinhole degassing system. *Journal of the Acoustical Society of America*, 99:3857–3860, 1996.

[45] K.S. Spratt, K.M. Lee, P.S. Wilson, and M.S. Wochner. On the resonance frequency of an ideal arbitrarily shaped bubble. *Journal of the Acoustical Society of America*, (134):4061, 2013.

[46] K.S. Spratt, K.M. Lee, P.S. Wilson, and M.S. Wochner. On the resonance frequency. *Proceedings of Meetings on Acoustics*, 20, 2014.

[47] J. Borwick. *Loudspeaker and Headphone Handbook*. Focal Press, 3 edition, 2001.

[48] T.G. Leighton, P.R. White, C.L. Morfey, J.W.L. Clarke, G.J. Heald, H.A. Dumbrell, and K.R. Holland. The effect of reverberation on the damping

of bubbles. *Journal of the Acoustical Society of America*, 112:1366–1376, 2002.

[49] T.F. Argo IV, P.S. Wilson, and V. Palan. Measurement of the resonance frequency of single bubbles using a laser Doppler vibrometer. *Journal the Acoustical Society of America Express Letters*, 123:121–125, June 2008.

[50] C.N. Dolder. Fish school acoustics. Ph.D. Dissertation, The University of Texas at Austin, 2014.

Vita

Gregory Robert Enenstein was born and raised in the San Francisco Bay Area. He received a Bachelor of Science degree in Mechanical Engineering from Stanford University in 2010. After working 2 mechanical engineering jobs, he decided pure mechanical engineering was not his true passion. Rather, he wanted to incorporate sound into his engineering career, which is how he ended up studying acoustics. For him, music had always been an integral part of his life. Starting with 11 years of classical piano lessons and then singing in the Stanford Mendicants, Stanford's oldest a cappella group, Greg has had a rich experience with music. Since then he has focused on classic rock, power pop, and indie styles, playing bass, guitar, and singing in several bands, eventually playing at SXSW music festival. After completion at the University of Texas, Greg hopes to immerse himself in the field of architectural acoustic consulting. But first a trip to Europe is in order.....

Email address: gregenenstein@gmail.com

This thesis was typeset with LaTeX[†] by the author.

[†]LaTeX is a document preparation system developed by Leslie Lamport as a special version of Donald Knuth's TeX Program.